DOI: https://doi.org/10.1016/j.oceaneng.2021.108971

Behavior of Concrete Modular Multi-Purpose Floating Structures

D. Jiang[1], K.H. Tan[2], J. Dai[3], K.K. Ang[2], and H.P. Nguyen[4]

[1]Department of Civil Engineering, School of Science, Nanjing University of Science and Technology, Nanjing 210094, China
[2]Department of Civil and Environmental Engineering, National University of Singapore, Kent Ridge, Singapore 119260
[3]Department of Civil Engineering and Energy Technology, Oslo Metropolitan University, Oslo 0166, Norway
[4]School of Civil Engineering, University of Queensland, St Lucia, Queensland 4072, Australia

ABSTRACT

Large floating structures such as platforms, breakwaters and piers, have been constructed in many countries in coastal areas in a bid to increase land space. Due to construction ease and operational flexibility, these facilities are commonly consisted of relatively small floating units that are subsequently connected on sea. This paper first describes box-like structural systems for concrete floating structures. Finite element (FE) analyses are then performed to assess the structural performance of concrete floating structures when subjected to self-weight, imposed live load, hydrostatic pressure and buoyancy force. The effects of geometrical shapes, cell numbers and slab thickness on the structural performance of box-like floating modules are investigated. Results indicate the need to provide prestressing steels so as to prevent cracking in the concrete modules. Besides, material requirements for different configurations were compared to provide the most economical solution for box-like concrete floating units. Furthermore, global responses of modular multi-purpose floating structures with different geometrical shapes were investigated via hydroelastic analyses using self-developed hybrid boundary element (BE) – FE code. Global flexural stresses are found to be quite high for rigidly-interconnected large floating structures due to regular wave loadings, especially when the geometrical aspect ratio becomes large. The use of hinge joints is effective in reducing bending moments but it relatively increases the vertical deflections. A trade-off should be considered between internal loads and structural motions in the conceptual design of large floating structure system.

Keywords: Box-like Structure; Finite Element Analysis; Hydroelastic Analysis; Modular Multi-Purpose Floating Structures.

1. INTRODUCTION

For many large urban cities, there is a constant demand for more usable space to meet the developmental and economic needs of an ever increasing population. In this respect, the use of coastal sea space, where available, is a viable solution to address the issue of land scarcity. The use of floating structures is preferable to the convetional land reclamation that involves dumping sands/rocks into the sea. This is because it is more environmentally friendly and less time consuming in construction (Jiang et al., 2018; Wang et al., 2015). Moreover, the self-weight of floating structures is automatically balanced by the buoyancy force, thus eliminating the need for massive and expensive foundations, which in turn results in savings in material and construction costs. In the past decades, large floating structures such as platforms, breakwaters, piers and others, have been constructed in many countries (Dai et al., 2018; Jiang et al., 2017; Jiang et al., 2019; Wan et al., 2019). These facilities are commonly composed of relatively small floating modular units due to construction ease and operational flexibility. It is of interest to determine viable and economical structural solutions for floating modules.

The floating modular unit generally acquires sufficient upward buoyancy force by means of voided compartments. Currently, the applications of structural solutions and construction materials for floating modules vary from region to region. Back in 1980s, Yee developed the concrete honeycomb structural system, as shown in Figure 1a, and it has been applied in some engineering practices, such as the Rofomex floating dock and Densit floating barge (Fernandez and Pardo, 2013; Yee, 2009). This system employs a honeycomb sandwich design consisting of vertical cylindrical cells aligned in rows and connected to each other by thin concrete walls. The integration of precast concrete cylindrical components in combination with exterior side walls, top slab and bottom slab provides exceptional structural stiffness and strength with less amount of concrete, steel reinforcement and prestressing steels. However, the complex configuration of honeycomb structures generally makes the construction procedure time-consuming and costly.

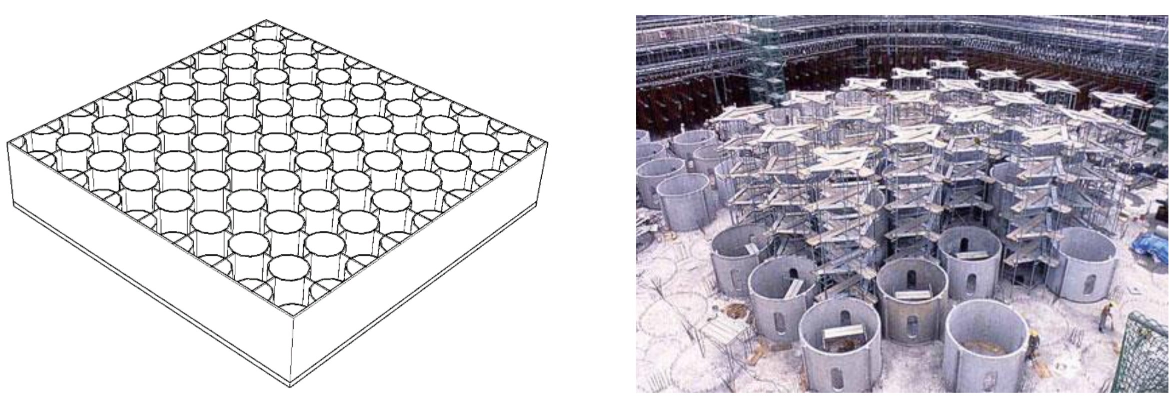

(a) Honeycomb structure layout (b) Honeycomb construction (Wang, 2015)

Figure 1. Honeycomb Structural Solution for Floating Units.

For military purposes, the Mobile Offshore Base (MOB) was developed to accommodate take-off and landing long-rang cargo aircraft, as shown in Figure 2 (Mcallister, 1997; Ramsamooj and Shugar, 2002; Rognaas et al., 2001). Several MOB conceptual designs were proposed with using different materials, such as steel, concrete or a combination thereof. Figure 2b shows a semi-submersible design of MOB, which consists of the concrete hull and steel topside. Rognaas et al., (2001) performed a comprehensive finite element (FE) anlsyis on the invidual MOB structure, where shell elements were utilized and the wave loads were generated by the commercial software WADAM and applied to the FE model. However, Rognaas et al., (2001) mentioned that the moment effects were not included in the FE analysis, which may influence the evalution of concrete portions.

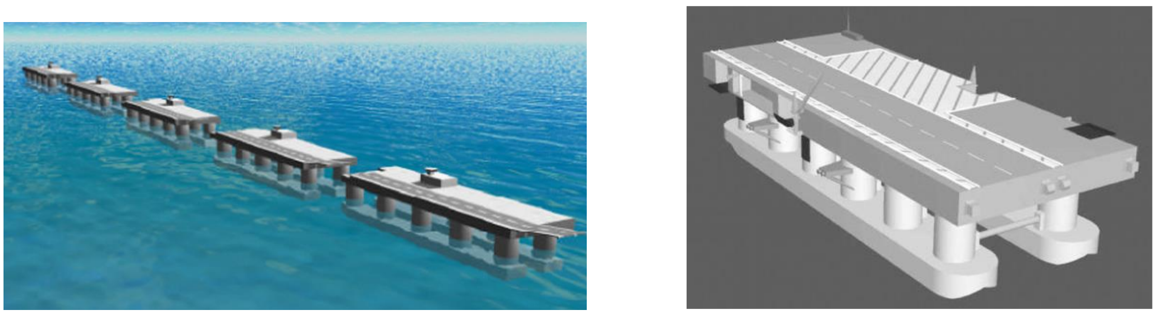

(a) MOB structure (Lamas-Pardo et al., 2015).   (b) Hybrid MOB modue (Rognaas et al., 2001)

Figure 2. Honeycomb Structural Solution for Floating Units.

Wong et al. (2013) and Dai et al. (2019) studied the use of high density polyethylene (HDPE) for constructing the floating wetlands and the floating modular photovoltaic panel system, respectively, as shown in Figure 3. Local stresses of the floating module is analysed with FE method where HDPE is treated as an isotropic materialBy simplifying the the entire floating structure as an equivalent Mindlin plate, hydroelastic analyses were performed to examine the moment and shear strength capcities.

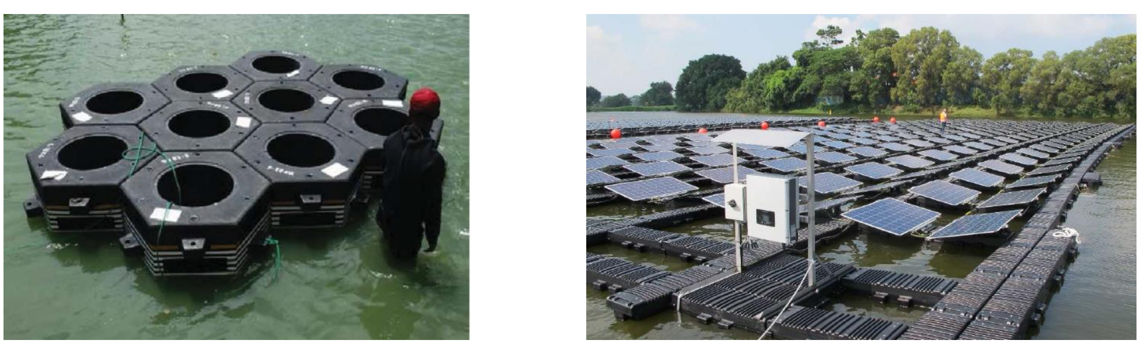

(a) Modular units for floating wetlands   (b) floating modular photovoltaic panel system

Figure 3. HDPE Floating Modular Structures (Wong et al., 2013; Dai et al., 2019).

Besides aforementioned structural solution alternatives, floating modules can also be made as boxes with different geometries and cell numbers. Figure 4a shows a rectangular box-like floating modular unit, in which the internal walls are used to increase the structural stiffness and reduce the flexural stresses in the top and bottom slabs. The Marina Bay floating platform in Singapore measures 120 m in length, 83 m in width and 1.2 m in depth and was built by assembling steel rectangular box-like modules. Wang and Tay (2011) focused on the hydroelastic analysis of the entire floating platform with assuming all the modules are connected rigidly, but no detailed analysis of the individual floating module was reported (Koh and Lim, 2009). Morris (1996) has filed a patent to show the conceptual design of an artificial prestressed concrete (PC) floating structure formed by a plurality of hexagonal and triangular cells, as shown in Figure 1b. The hexagonal shape structure has been adopted by architects as a basic unit for conceptual designs of floating cities (Seasteading Institute, 2020). However, no analysis work has been conducted to evaluate the structural performance of the PC hexagonal modules and the entire floating structutres.

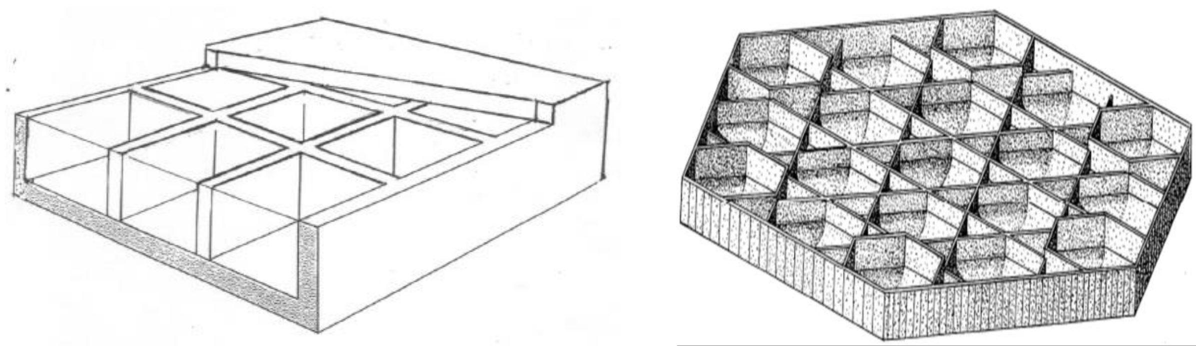

(a) Rectangular shape (b) Hexagonal shape (Morris, 1996)

Figure 4. Box-like Structural Solutions for Floating Units.

Engineering practices indicate that floating structures can be made of various materials. However, when properly designed and constructed under strict quality control, concrete would be a preferred material for modular floating structures in the seawater environment because of some key advantages (Fernandez and Pardo, 2013; Priedeman and Anderson, 1985): (1) the use of concrete material generally results in a lower initial construction cost; (2) concrete shows superior durability in the seawater environment, which shall reduce the costs for maintenance, inspection and repair; (3) concrete structures have larger local and global stiffness, and show better performances in withstanding accidental impact loads; (4) large floating concrete structures can be assembled with precast components integrated by post-tensioning (P.T.) tendons, leading to an easier construction. The concrete itself is a brittle material that is strong in compression but very weak in tension, thus the analysis and design of concrete structures differ from structures made of isotropic materials. Additionally, prestressing steels are commonly used to achieve reliable structural concrete designs, and the degree of prestressings often determined by counteracting the load effect of dominant actions such that no tensile stresses exist in the critical section. Up to present, most scholars focused on hydroelastic response analysis of large floating structures to determine the global deflection and stresses, considering the modular structure as a rigid unit (Fu et al., 2007; Loukogeorgaki et al. 2012). Limit research work on the structural behavior of the floating module itself was reported, especially for the prestressed concrete modular floating structures.

In this paper, the structural behaviour of concrete box-like floating modules are evaluated using the FE analysis, and the effects of geometrical shapes, cell numbers and slab thickness are investigated. Besides, material requirements for different configurations of box-like structures are compared to determine the most economical solution for concrete floating modular units. Moreover, global responses of large floating structures composed of selected modular structures with different geometrical shapes are investigated by performing hydroelastic analysis using a self-developed hybrid boundary element (BE)-FE code. Last, suggestions and recommendations on the design of modular floating structures are provided for the engineering practice.

2. DESIGN ALTERNATIVES FOR CONCRETE FLOATING MODULES

Considering the ease of construction and installation, relatively small sizes of floating modules are selected in the conceptual designs. For the rectangular module, the length, width and height are set as 30 m, 15 m and 5 m, respectively, as a benchmark. Table 1 lists the plan dimensions of different geometrical shapes that have the same plan area as the benchmark rectangular shape. It can be seen that the hexagonal shape has the smallest perimeter, which indicates that it requires the least volume of concrete for the same wall thickness and height. It should be mentioned that the listed possible shapes and sizes were chosen in the conceptual development based on a set of selection criteria, which include the construability, ease of connection, preliminary structural and hydrodynamic performance, and cost-effectiveness (Ang et al., 2020; Ren et al., 2019; NUS and SINTEF, 2019). In this study, rectangular and hexagonal shapes will be selected for further structural evaluations.

Table 1. Dimensions of Different Geometrical Shapes.

Geometrical Shape	Dimensions	Perimeter
<u>Rectangle</u>	<u>30 m × 15 m</u>	<u>90 m</u>
Regular Triangle	Side length: 32.2 m	96.7 m
Square	Side length: 21.2 m	84.9 m
Regular Pentagon	Side length: 16.2 m	80.9 m
<u>Regular Hexagon</u>	<u>Side length: 13.2 m</u>	<u>79.0 m</u>

Note: underscore items denote geometrical shapes selected for further structural evaluations.

Table 2 lists all box-like floating modules investigated in this study. The variable parameters include geometrical shape, cell numbers and wall/slab thickness. For the rectangular modules, 1-cell, 2-cell and 4-cell structures are considered. For the hexagonal modules, 1-cell, 6-cell, 7-cell and 24-cell structures are considered. For each case, the wall thickness, and the top and bottom slab thickness are kept the same, and varied as 150 mm, 225 mm and 300 mm.

Table 2. Variable Parameters for Rectangular and Hexagonal Modules.

Shape	**No. of Cells**	
Rectangle	1-cell	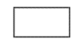
	2-cell	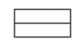
	4-cell	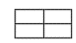
Regular Hexagon	1-cell	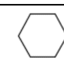
	6-cell	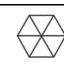
	7-cell	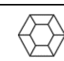
	24-cell	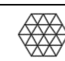

3. STRUCTRAL ANALYSIS AND PRESTRESSING DESIGN

3.1 Finite Element Modelling

In this study, FE models are developed for different types of floating modules using the commercial software ABAQUS. Figure 5 shows FE models of representative box-like floating modular structures. Solid element (C3D8R) was used in the analysis to model concrete structural components , and the C3D8R element is a general purpose linear eight-node solid element with three degrees of freedom at each node.Compared to the shell element, the solid element can represent the structural geometries more realistically and allow reinforcing and non-reinforcing steel elements to be easily embedded in the structure model at a later stage. The mesh of each model was generated with evenly spaced nodes in plane, and at least three nodes were uniformly distributed in the direction of slab thickness. For the purpose of finding the optimum mesh size, several models with different mesh sizes (100 mm, 200 mm, and 500 mm) were investigated in one specific load case for the critical transverse path along the top slab in the 2-cell rectangular module. Figure 6 presents the flexural stress distributions along path 1-2 with different mesh sizes. As the figure illustrates, the computational results converged as the mesh size became smaller. Although the analyses demonstrated satisfactory outcomes could be achieved with the 200 mm mesh, the finer 100 mm mesh was adopted as the additional modeling and computational effort was not significant. Both reinforcing and prestressing steels were modelled as truss elements (T3D2) and embedded into the concrete section, which assumes full bond interaction between two materials. The floating modules are designed to remain in the linear elastic range of behavior at the serviceability limit state (SLS) by using prestressed concrete. As such, a linear elastic model can be defined. Also, the density of lightweight concrete was taken as 2000 kg/m^3.

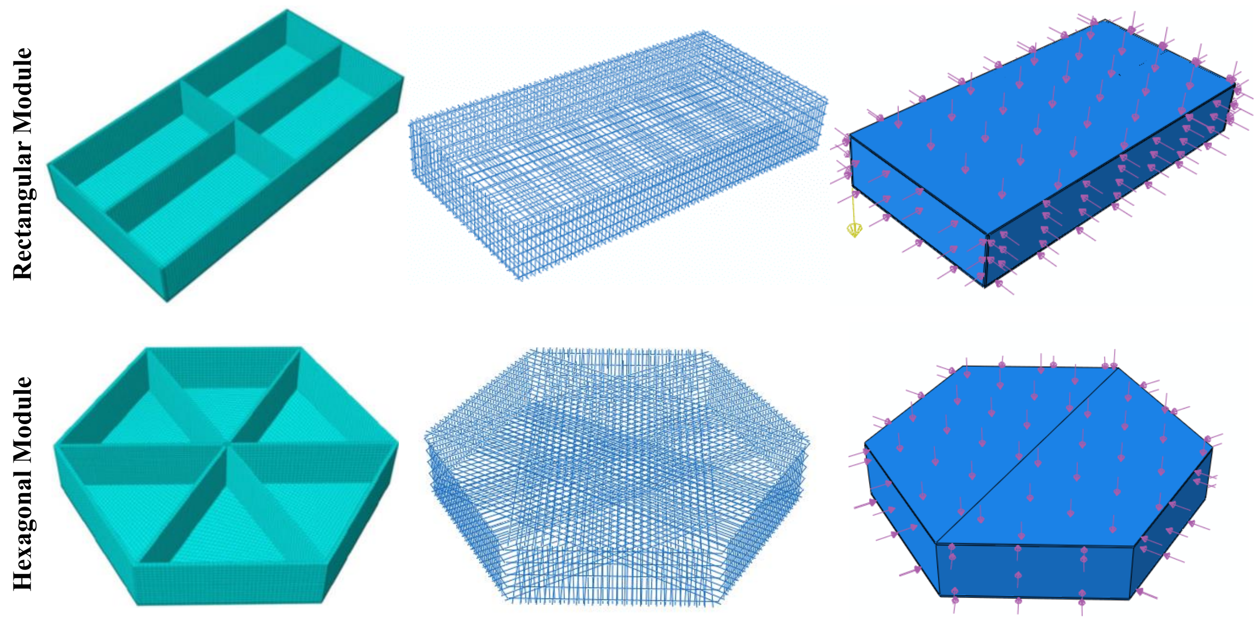

(a) Concrete Components (b) Prestressing Steels (c) Load Application

Figure 5. Finite Element Models of Different Floating Modules

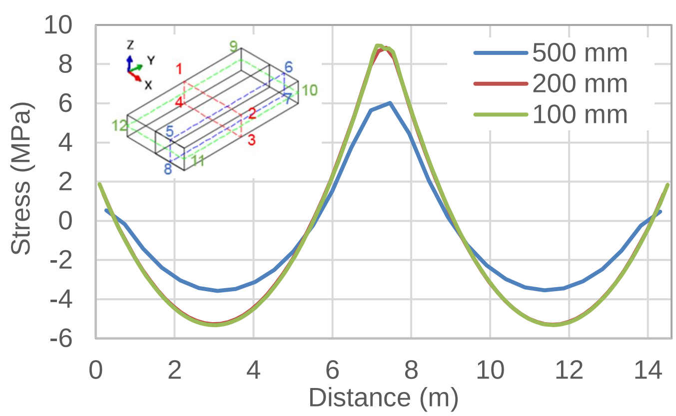

Figure 6. FEM Mesh Sensitivity Analysis for 2-Cell Rectangular Module.

The floating modular structures are subjected to various actions under service conditions, for example, self-weight, hydrostatic pressures, wave load, current load, wind load, and others. Previous experience indicates that hydrostatic pressure generally contributes a major proportion of the action effects compared to the other actions. Therefore, only the self-weight, imposed live load (5 kN/m^2) and hydrostatic pressures are taken into consideration in the FE analysis to evaluate the structural performance of different floating modules. Figure 7 depicts the load patterns applied on the floating module. The hydrostatic pressures due to seawater are determined using

$p_w = \rho_w g h_w$, where the density of seawater, ρ_w, is taken as 1025 kg/m^3, and h_w is the seawater draft. The hydrostatic pressure around the floating modular structure is automatically balanced because of the geometric asymmetry. Linear springs are attached beneath the base slab to simulate the upward buoyancy effects and also act as the boundary conditions, which can automatically account for the varying pressure due to bottom slab deflections. The spring constant for unit area of the bottom slab is taken as $k_s = \rho \cdot g$ = 10055 N/m^3. Draft values for each floating module are determined by balancing the upward buoyancy force with downward load effects, as shown in Figure 7. It is observed from Table 3 that draft values are slightly different for various floating modules, which results from different magnitude due to self-weight. For each floating module, stress distributions are extracted to check the allowable stress limits at SLS and the necessity for prestressing steels is evaluated.

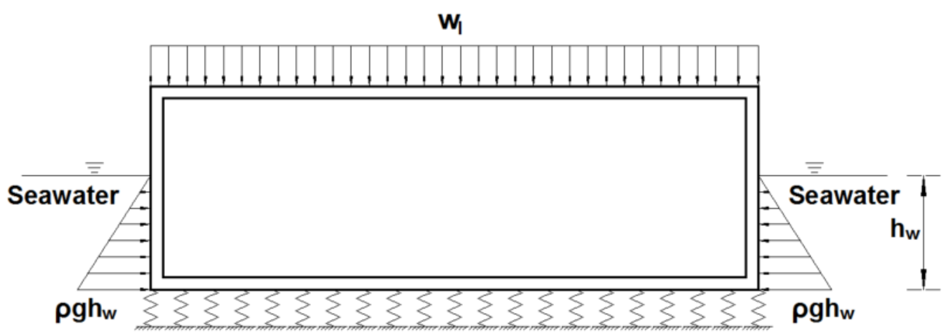

Figure 7. Hydrostatic Pressures Applied on the Floating Module.

Table 3. Seawater Drafts and Pressures for Different Floating Modules.

Shape	No. of Cells	Thickness (mm)	Seawater Draft (m)	Hydrostatic Pressure (kPa)
Rectangle Box-like Structure	1-cell	150/225/300	1.36/1.77/2.23	13.7/17.8/22.4
	2-cell	150/225/300	1.45/1.90/2.41	14.6/19.1/24.2
	4-cell	150/225/300	1.49/1.97/2.51	15.0/19.8/25.2
Regular Hexagon Box-like Structure	1-cell	150/225/300	1.29/1.68/2.09	13.0/16.9/21.0
	6-cell	150/225/300	1.53/2.02/2.58	15.4/20.3/25.9
	7-cell	150/225/300	1.53/2.02/2.58	15.4/20.3/25.9
	24-cell	150/225/300	1.83/2.52/3.30	18.4/25.3/33.2

3.2 Analysis Results

Flexural stress distributions are taken along different paths of box-like structures to identify the critical stress values and evaluate the requirement for prestressing steels. Figure 8 shows the three paths, 1-2-3-4, 5-6-7-8, and 9-10-11-12, taken in the longitudinal, transverse and vertical directions, respectively, for rectangular box-like modular units. Paths are purposely selected at the middle section between two adjacent supports, where the maximum stresses are expected. Figure 9 presents paths for stress evaluation in hexagonal box-like modular units. The paths 1-2-3-4 and 5-6-7-8 are taken along the short and long side of both the top and bottom slabs, while path 9-10 is taken along a side wall.

Rectangular Modular Units

Figure 10 shows typical flexural stress distributions for a 2-cell module. The red, blue, and grey lines are for modular units with slab and wall thickness of 150 mm, 225 mm and 300 mm, respectively. The positive values indicate tensile stresses, while the negative values indicate compressive stresses. It can be seen that the top and bottom slabs of all modules deflect inwards, while side walls bulge outwards, which can be attributed to the large intensity of downward imposed live load and upward buoyancy effects. The flexural stresses reduce with the increase in slab/wall thickness and cell numbers, which attributes to the larger plate flexural rigidity and shorter span length between adjacent internal walls. For different modular structures, the maximum stress in the top and bottom slabs always occurs along paths 1-2 and 3-4 between two adjacent supports, which is due to one-way action of the slabs having a length/width ratio more than 2. Figure 11 presents the maximum tensile and compressive stresses for different cell numbers and slab/wall thicknesses. The compressive stresses are generally within the allowable compressive stress (f_{cd} = 30 MPa for C45/55). However, the tensile stresses at critical locations exceed the allowable tensile stress (f_{ctd} = 1.80 MPa for C45/55), which necessitates the provision of prestressing steels to reduce the tensile stresses. Note that the design compressive and tensile stress limits are determined by $f_{cd} = \alpha_{cc} f_{ck} / \gamma_c$ and $f_{ctd} = \alpha_{ct} f_{ck,0.05} / \gamma_c$ based on Eurocode EN 1992-1-1, where α_{cc} and γ_c are taken as 1.0 and 1.5 respectively. It is worth mentioning that negative moments exist at locations of end and interior wall supports, resulting in high tensile stresses, but these can be mitigated by chamfering technique at the joints.

Hexagonal Modular Units

Figure 12 shows the flexural stress distributions along various paths for a 6-cell module, representative of hexagonal modular units. The legend for the colored lines and stress sign convention are the same with Figure 10. Similar to rectangular modules, the top and bottom slabs are found to deflect inwards, while side walls bulge outwards. Smaller stress magnitudes are observed with increased slab/wall thicknesses and relatively shorter spans between adjacent vertical wall supports.

Figure 13 presents the maximum tensile and compressive stress values in different hexagonal floating modules with different cell numbers and slab/wall thicknesses. An interesting phenomenon is that the stress magnitude of the 7-cell module is larger than that of 6-cell module, which can be attributed to a relatively larger span in the inner hexagon. Compressive stresses are generally within the allowable compressive stress (f_{cd} = 30 MPa for C45/55). Maximum tensile stresses of only four cases, that is, 6-cell (300 mm) and 24-cell (150/225/300 mm), satisfy the design tensile stress limit (f_{ctd} = 1.80 MPa for C45/55). It is concluded that the prestressing steels are generally needed for most hexagonal floating modules. Specifically, no necessity for prestressing steels in the 24-cell module is attributed to a much shorter span in the inner hexagon, but its complex configuration makes the construction procedure time-consuming and costly.

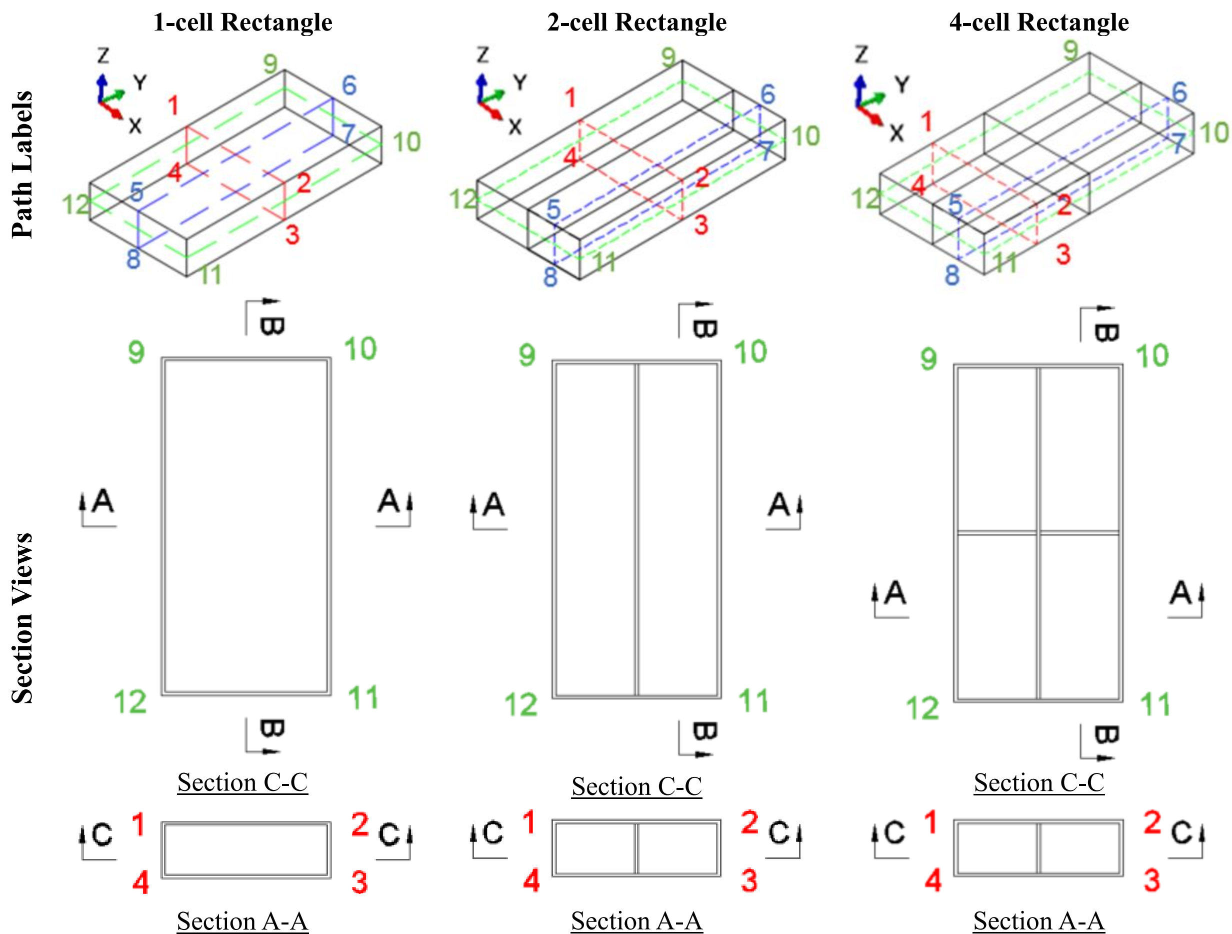

Figure 8. Various Paths for Stress Extraction (Rectangular Box-like Structures).

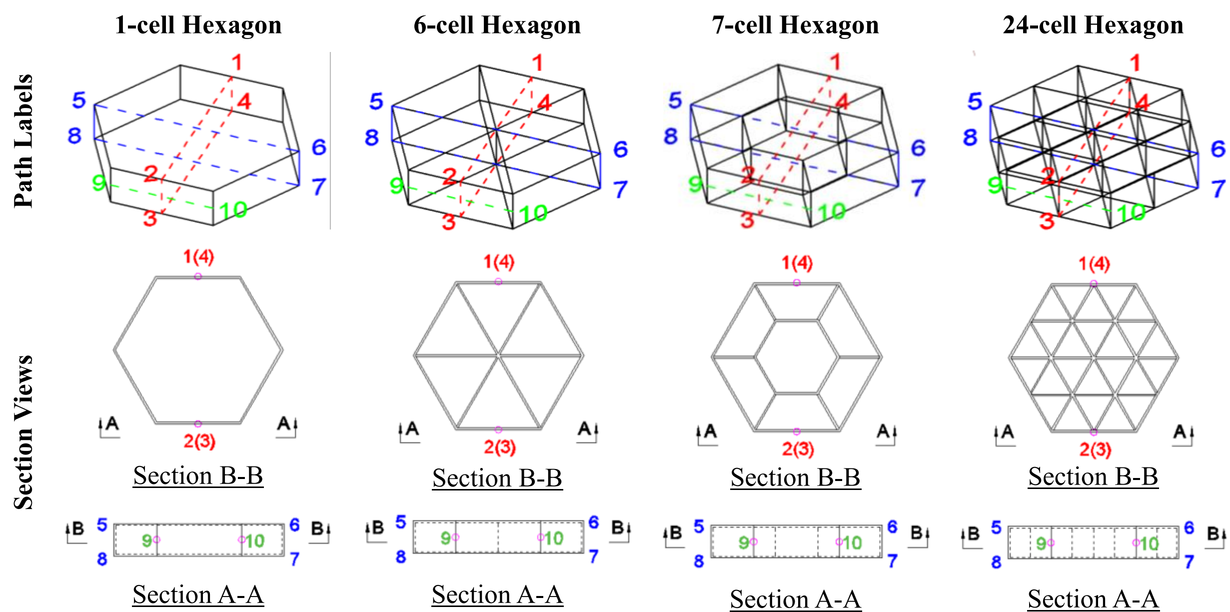

Figure 9. Various Paths for Stress Extraction (Hexagonal Box-like Structures).

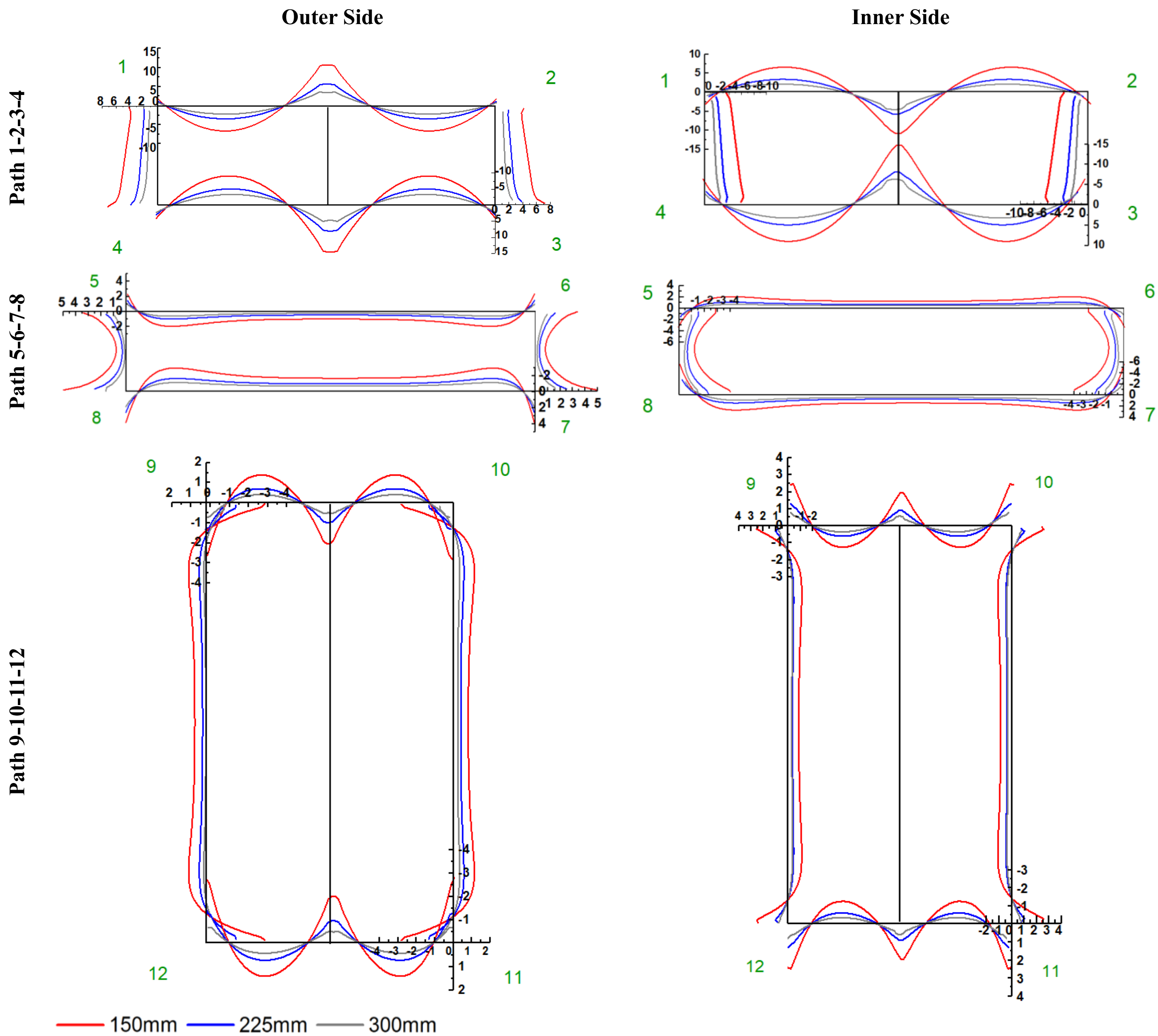

Note: All values of stress are in MPa.

Figure 10. Stress Distribution in 2-cell Rectangular Box-like Floating Modular Structure.

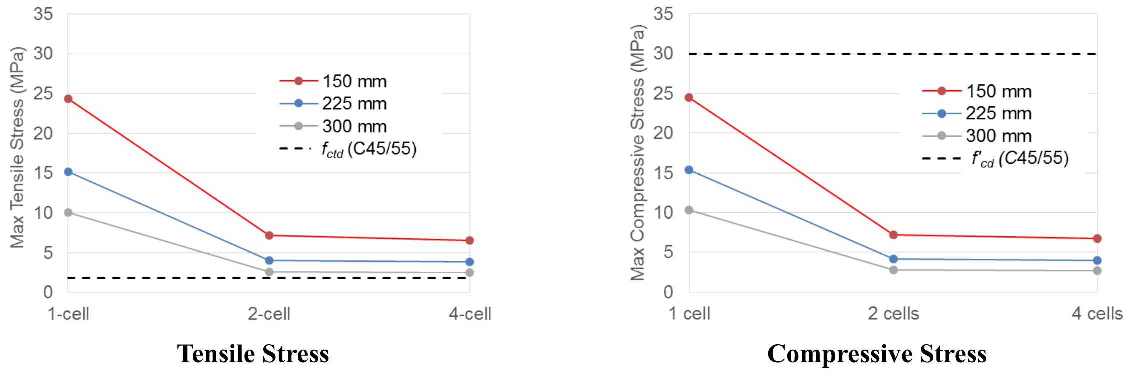

Figure 11. Comparison of Maximum Flexural Stresses in Rectangular Box-like Modules.

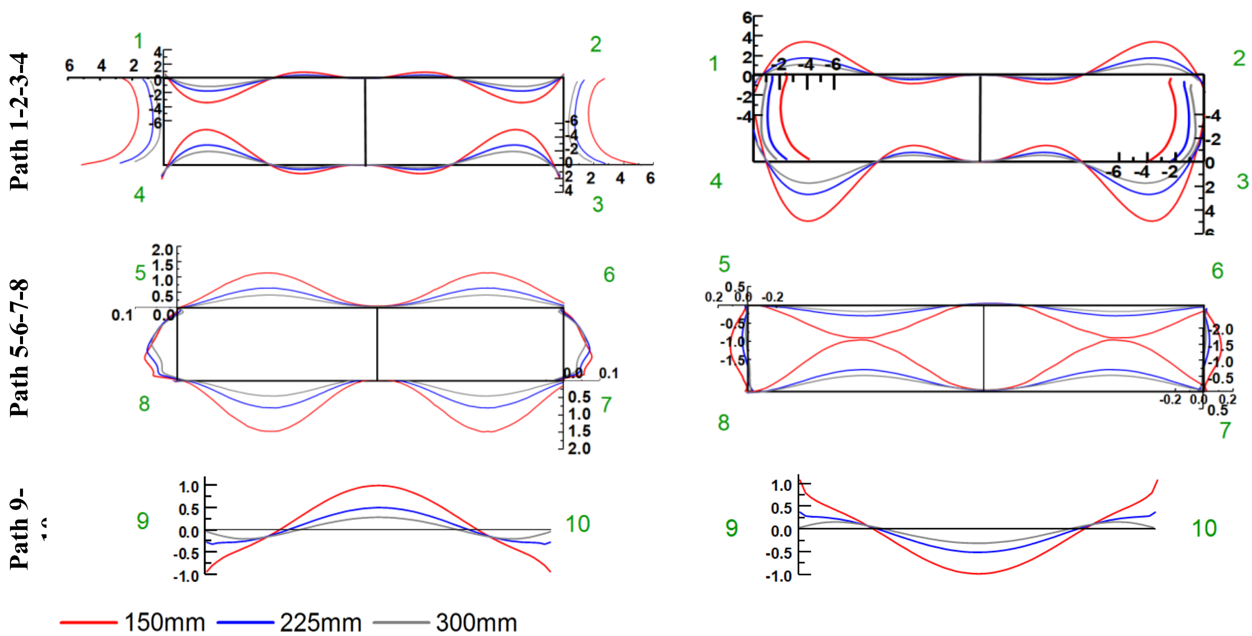

Note: All values of stress are in MPa.

Figure 12. Stress Distribution in 6-cell Hexagonal Box-like Floating Modular Structure

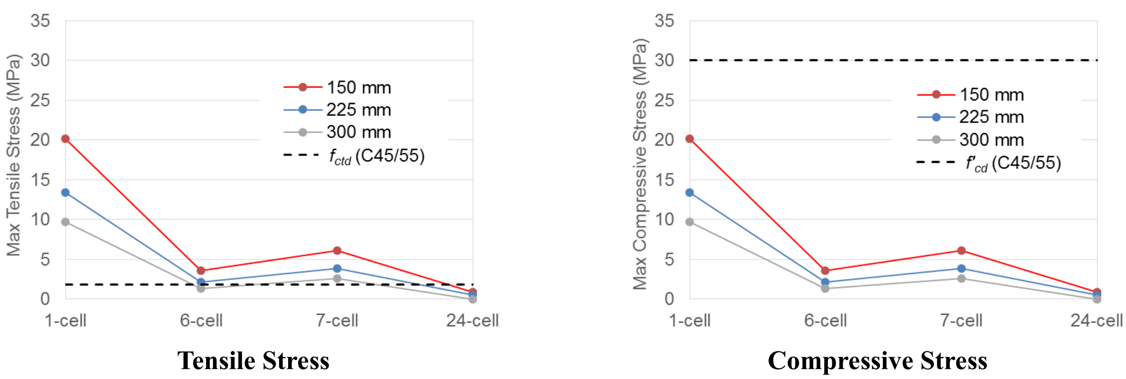

Figure 13. Comparison of Maximum Flexural Stresses in Hexagonal Box-like Modules.

3.3 Preliminary Design of Prestressing Steels

In order to counteract the tensile stresses, prestressing steels are applied in the box-like floating modules to keep the concrete at an uncracked state. When the prestressing steels are embedded inside the modular structures, the generated compression effect is considered to be uniform across the thickness of thin slabs and walls. The amounts of prestressing steels can be simply designed to counteract the tensile stresses according to the equation $\sigma_t \cdot t \cdot h = A_{ps} \cdot f_{ps}$, where σ_t is the tensile stress that needs to be eliminated, t is the slab/wall thickness, h is the unit slab/wall width, taken as 1000 mm, A_{ps} is the required areas of prestressing steels per metre width, f_{ps} is the effective stress after considering prestressing losses, taken as 1100 MPa. Design parameters for prestressed concrete floating modules are based on the standard practice. The concrete grade is specified to be C45/55, and the allowable compressive stress, f_{cd}, and the allowable compressive stress, f_{ctd}, are 30 MPa and 1.80 MPa, respectively. The standard prestressing steels used herein is 12.7 mm diameter low relaxation strands with the ultimate strength, f_{pu}, of 1860 MPa. In order to achieve an economical design, the amounts of prestressing steels are designed differently for side walls, top slab and bottom slab according to the tensile stress magnitudes. FE analysis was also performed on the modular structures after prestressing steels are incorporated. In the ABAQUS program, prestressing steels were modelled as truss elements and embedded in concrete solid elements. Figures 14 and 15 show the stress distribution of 2-cell rectangular and 6-cell hexagonal box-like modules after applying the prestressing steels. It is observed that the stress curves shift towards the compression side, and all tensile stresses have been balanced by the prestressing forces.

3.4 Evaluation of Various Design Alternatives

Based on the preliminary prestressing designs, material costs for various design alternatives are determined. In the calculation, the cost of concrete is taken as SGD$135 per m^3 while the cost of steel is taken as SGD$900 per tonne. Figure 16 shows the cost comparisons of floating modules with or without prestressing steels. It is observed that total material costs generally decrease with smaller slab/wall thickness values. The prestressing steel amount is reduced to the extent that the 24-cell hexagonal module does not require any prestressing steel to satisfy the stress check. However, the 24-cell hexagonal module becomes too complex for construction. On the other hand, for the rectangular modules, the cost for the 4-cell rectangular module is slightly higher than that of the 2-cell rectangular module. For the optimal solution to be achieved, similar slab and wall thicknesses are adopted for both models, which results in more reinforced concrete being used for the 4-cell rectangular module.

In summary, the 2-cell rectangular module and the 6-cell hexagonal module give the most economical solution. Hence, the prestressed concrete 2-cell rectangular module, and prestressed concrete 6-cell hexagonal module, both with 150 mm thick walls and slabs, are preferable structural solutions as they satisfy the allowable stress check and are the most economical design. These two modular structures will be selected to compose large floating structures and further analysis the hydroelastic responses, which will be described in the next section.

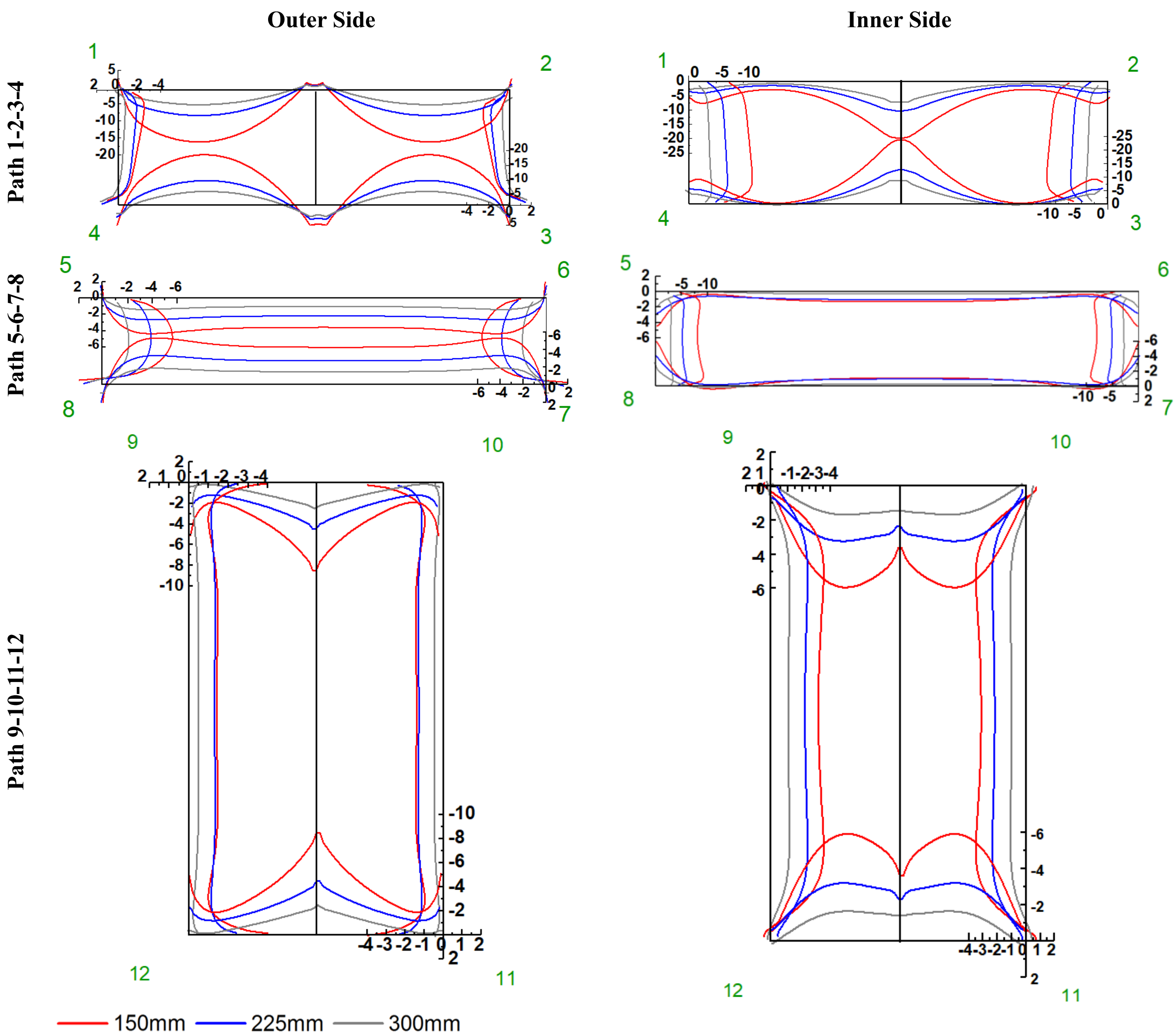

Note: All values of stress are in MPa.

Figure 14. Stress Distribution along Different Paths in 2-cell Rectangular Box-like Floating Modular Structure after Applying Internal Prestressing Steels.

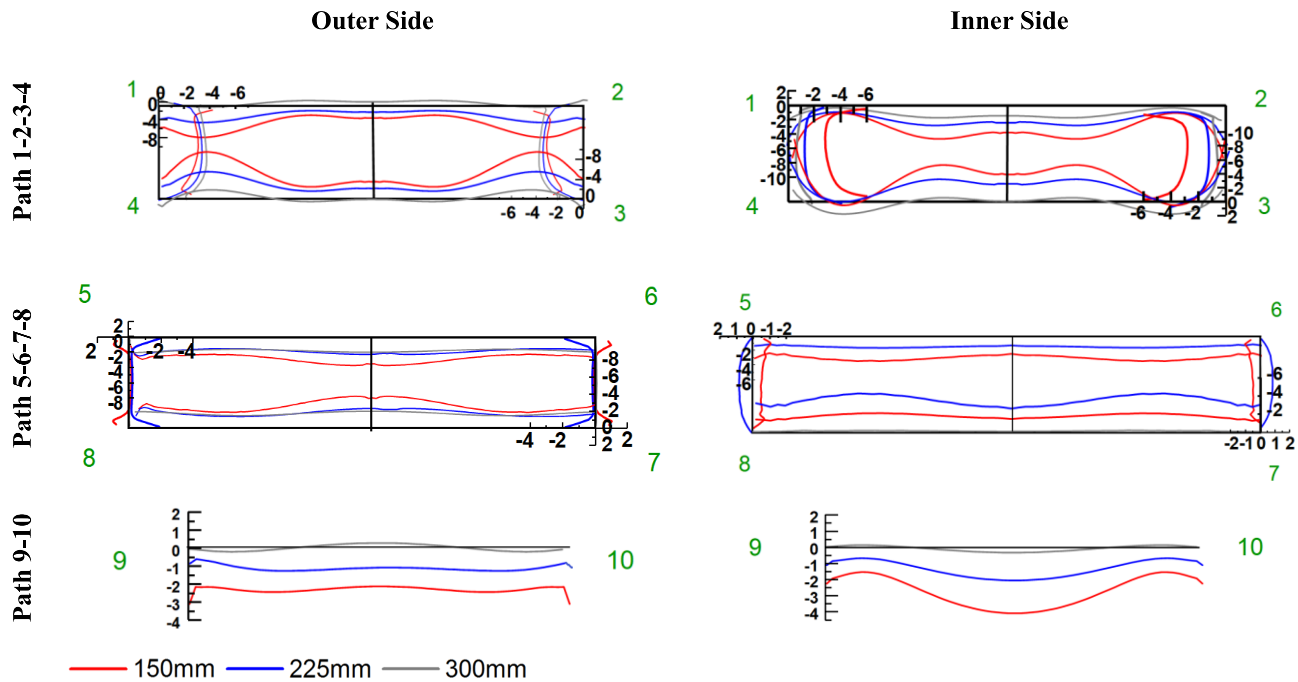

Note: All values of stress are in MPa.

Figure 15. Stress Distribution along Different Paths in 6-cell Hexagonal Box-like Floating Modular Structure

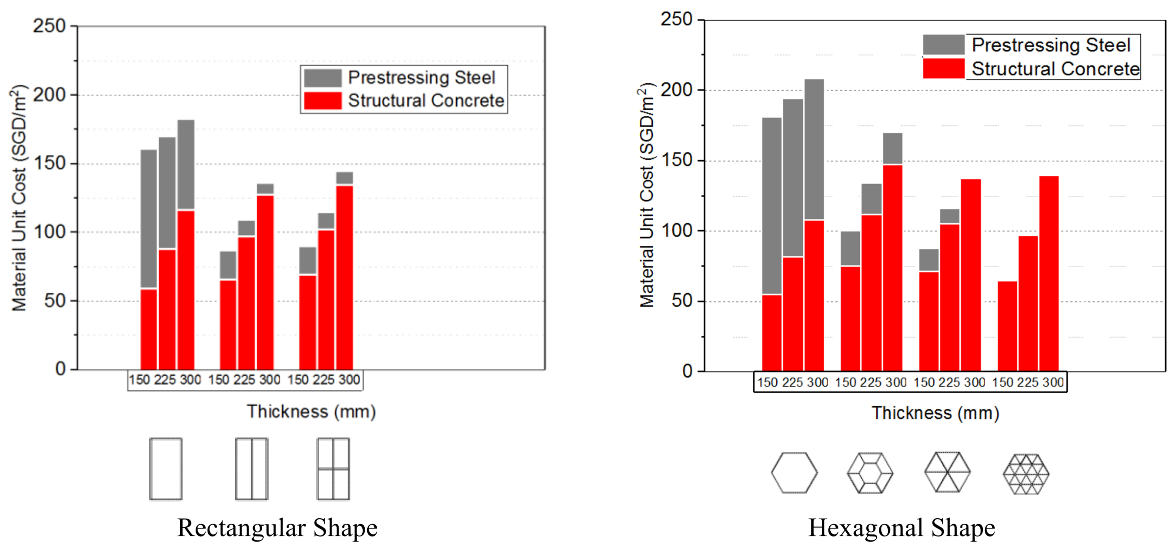

Figure 16. Cost Comparisons for Different Floating Modules.

4. HYDROELASTIC RESPONSE OF INTERCONNECTED FLOATING STRUCTURES

When the entire floating structure is assembled with modular units, load situations will become more complex than those shown in Figure 7. Particularly for floating structures with larger horizontal dimensions compared to the depth and the ocean wavelength, the hydroelastic responses are of concern because the flexural rigidity is relatively small and the elastic deformations are more important than the rigid-body motions (Wang and Tay, 2011).

Figure 17 presents a conceptual design for large floating structures. The mooring dolphin system is constructed to restrain horizontal movement of the structure but allow the VLFS to move up and down freely. In this section, hydroelastic responses of modular floating structures under regular waves in Singapore coastal water with water depth H = 20 m are discussed.

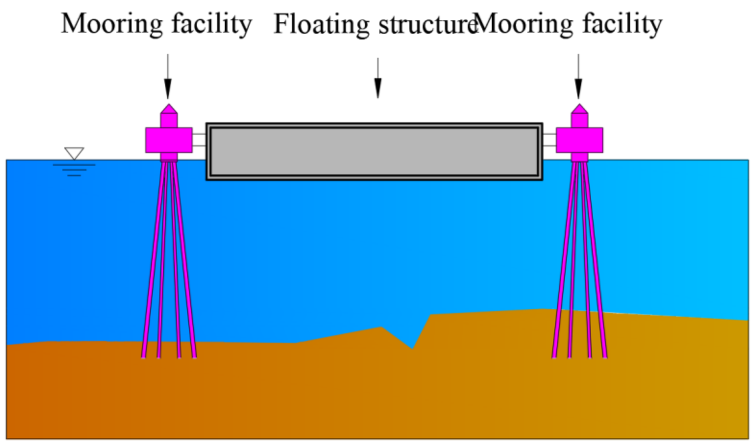

Figure 17. Conceptual Design for VLFS.

4.1 Methodology of Hydroelastic Analysis

Figure 18 depicts the box-like VLFS with the length of L, the width of B, and the height of h. The structure is subject to an incident wave with velocity potential ϕ_I , a circular frequency ω, wavelength λ, wave height 2A and wave angle θ with respect to x-axis. Massive degrees of freedom will be generated if one develops a detailed model for an actual VLFS composed of prestressed concrete floating modules, which makes hydroelatic analysis very costly and computational expensive. Under such circumstance, the detailed VLFS model is usually replaced with an equivalent solid Mindlin plate by keeping the geometric dimensions the same as the actual structure but the density ρ and Young's modulus E of the equivalent plate are tweaked to match the vibration modes and natural frequencies of the actual structure. The equivalent plate is assumed to be flat with free edges, which is restrained by the station keeping system in the x-y plane. The simplification of equivalent Mindlin plate have been validated by comparing hydroelastic responses with experimental test results (Tay et al., 2009; Utsunomiya et al., 1998; Wang and Tay, 2011). Moveover, this approach has been successfully implemented in the analysis and design of Marina Bay floating performance stage in Singapore (Wang, 2015).

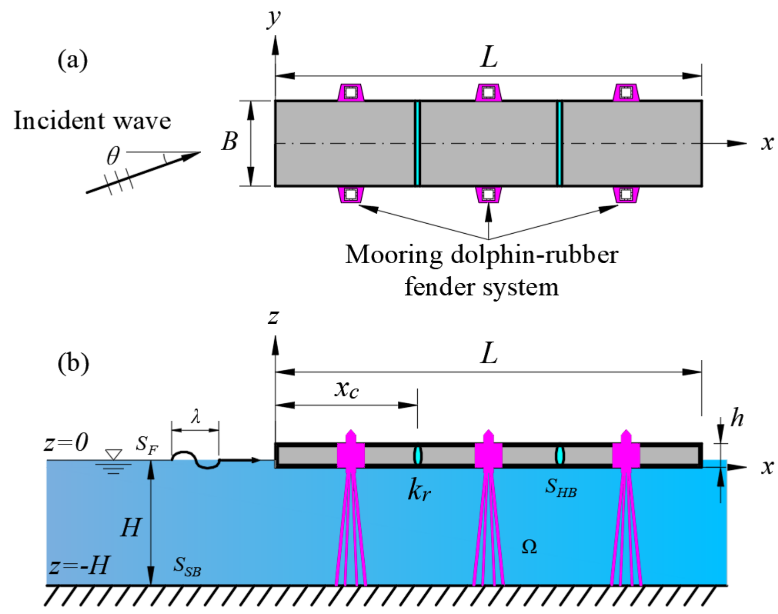

Figure 18. Coupled Structure–Water Problem: (a) Plan View and (b) Elevation View.

The hybrid BE-FE numerical approach is used to perform hydroelastic analyses in the frequency domain, where the finite element method is used to handle the equation of motion of the floating plate while the boundary element method is to solve the Laplace equation and the boundary conditions for the fluid part. The use of line connection is located at x_c from the fore of the VLFS as shown in Figure 18, which are indicated by cyan shaded strips. The governing equations of motion for the Mindlin plate (after omitting the time factor $e^{-i\omega t}$) are as follows:

$$\kappa^2 Gh\left[\left(\frac{\partial^2 w}{\partial x^2}+\frac{\partial^2 w}{\partial y^2}\right)+\left(\frac{\partial \psi_x}{\partial x}+\frac{\partial \psi_y}{\partial y}\right)\right]+\omega^2\rho_p hw=p(x,y), \tag{1}$$

$$D\left[\frac{(1-\nu)}{2}\left(\frac{\partial^2 \psi_x}{\partial x^2}+\frac{\partial^2 \psi_x}{\partial y^2}\right)+\frac{(1+\nu)}{2}\left(\frac{\partial^2 \psi_x}{\partial x^2}+\frac{\partial^2 \psi_y}{\partial x \partial y}\right)\right]-\kappa^2 Gh\left(\frac{\partial w}{\partial x}+\psi_x\right)+\omega^2\rho_p\frac{h^3}{12}\psi_x=0, \tag{2}$$

$$D\left[\frac{(1-\nu)}{2}\left(\frac{\partial^2 \psi_y}{\partial x^2}+\frac{\partial^2 \psi_y}{\partial y^2}\right)+\frac{(1+\nu)}{2}\left(\frac{\partial^2 \psi_y}{\partial y^2}+\frac{\partial^2 \psi_x}{\partial x \partial y}\right)\right]-\kappa^2 Gh\left(\frac{\partial w}{\partial y}+\psi_y\right)+\omega^2\rho_p\frac{h^3}{12}\psi_y=0, \tag{3}$$

where the motion is represented by the vertical displacement $w(x,y)$, the rotation $\psi_x(x,y)$ about the y-axis and the rotation $\psi_y(x,y)$ about the x-axis; κ^2 is the shear correction factor taken as 5/6; $G = E/[2(1+\nu)]$ is the shear modulus; $D = Eh^3/[12(1-\nu^2)]$ is the flexural rigidity; ω is the circular frequency of the incident wave and $p(x, y)$ is the water pressure comprising the hydrostatic and hydrodynamic pressure, expressed as $p(x,y)=i\omega\rho_w\phi(x,y,0)-\rho_w gw$; ρ_w is the mass density of water; g is the gravitational acceleration and $\phi(x,y,0)$ is the velocity potential of water. The boundary conditions of the Mindlin plate with free edges require that the bending moments, twisting moments and shear forces must vanish at the edges, which are expressed as follows:

Bending moment $M_{nn} = D\left[\frac{\partial \psi_n}{\partial n} + \nu \frac{\partial \psi_s}{\partial s}\right] = 0$ (4)

Twisting moment $M_{ns} = D\left(\frac{1-\nu}{2}\right)\left[\frac{\partial \psi_n}{\partial s} + \frac{\partial \psi_s}{\partial n}\right] = 0$ (5)

Shear force $Q_n = \kappa^2 Gh\left[\frac{\partial w}{\partial n} + \psi_n\right] = 0$ (6)

where the subscripts n and s denote the normal and tangential directions, respectively. At the connection, the continuity equations for the floating plate are

$$w\Big|_{x=x_c^-} = w\Big|_{x=x_c^+} \tag{7}$$

$$\psi_y\Big|_{x=x_c^-} = \psi_y\Big|_{x=x_c^+} \tag{8}$$

$$M_x\Big|_{x=x_c^-} = M_x\Big|_{x=x_c^+} = k_r\left(\psi_x\Big|_{x=x_c^+} - \psi_x\Big|_{x=x_c^-}\right) \tag{9}$$

$$M_{xy}\Big|_{x=x_c^-} = M_{xy}\Big|_{x=x_c^+} \tag{10}$$

$$Q_x\Big|_{x=x_c^-} = Q_x\Big|_{x=x_c^+} \tag{11}$$

where k_r is rotational spring stiffness of the connection. For a hinge line connection where the bending moment about y-axis is zero, $k_r = 0$. For a rigid connection, $k_r \rightarrow +\infty$. The continuity requirements given in Eqs. 7-11 are implemented into plate elements at the connection locations using the penalty method (Gao et al., 2011). According to the penalty method, if two points along the x-direction in the FE discretized model are connected to each other via a linear spring with rotational stiffness k_r, the global stiffness **K** needs to be modified as follows:

$$\mathbf{K}(l_3,l_3)_{new}=\mathbf{K}(l_3,l_3)+k_r \tag{12}$$

$$\mathbf{K}(k_3,k_3)_{new}=\mathbf{K}(k_3,k_3)+k_r \tag{13}$$

$$\mathbf{K}(k_3,l_3)_{new}=\mathbf{K}(k_3,l_3)-k_r \tag{14}$$

$$\mathbf{K}(l_3,k_3)_{new}=\mathbf{K}(l_3,k_3)-k_r \tag{15}$$

where the stiffness matrix **K** is obtained by following the standard finite element procedure; the subscript 'new' indicates the stiffness matrix that accounts for the connections between the l^{th} node and the k^{th} node; l_3 and k_3 indicate the degrees of fredoom corresponding to the rotations about y-axis at the l^{th} node and the k^{th} node. For other degrees of fredoom at the two nodes, a similar modification of the stiffness matrix is made, but for $k_r = \infty$.

The seawater is assumed to be an ideal fluid (that is, inviscid and incompressible) and the flow is irrotational so that the water motion can be modeled by a velocity potential. With these assumptions, the linear wave theory can be adopted for modelling fluid motions. According to this theory, the velocity potential ϕ must satisfy the following Laplace's equation and boundary conditions:

$$\nabla^2\phi(x,y,z)=0 \text{ in water domain} \tag{16}$$

$$\frac{\partial\phi}{\partial z}(x,y,0)=-i\omega w(x,y) \text{ on wetted surface} \tag{17}$$

$$\frac{\partial\phi}{\partial z}(x,y,0)=\frac{\omega^2}{g}\phi(x,y,0) \text{ on free surface} \tag{18}$$

$$\frac{\partial\phi}{\partial z}(x,y,-H)=0 \text{ on seabed} \tag{19}$$

$$\lim_{|\mathbf{x}|\to\infty}\sqrt{|\mathbf{x}|}\left(\frac{\partial(\phi-\phi_I)}{\partial|\mathbf{x}|}-ik(\phi-\phi_I)\right)=0 \text{ at far end} \tag{20}$$

where ϕ_I is the incident wave velocity potential, the free water surface has z = 0, and the seabed surface has $z = -H$.

By applying the Green's second identity to the Laplace's equation and the boundary conditions, we obtain the following boundary integral equation (Nguyen et al., 2018):

$$\phi(\mathbf{x})=\phi_I(\mathbf{x})+\int_{S_{HB}}G(\mathbf{x},\boldsymbol{\xi})\left[\frac{\omega^2}{g}\phi(\boldsymbol{\xi})+i\omega w(\boldsymbol{\xi})\right]\mathrm{d}\boldsymbol{\xi} \tag{21}$$

where **x** and **ξ** are the source point and the field point for water of finite depth. $G(\mathbf{x}, \boldsymbol{\xi})$ is the free surface Green's function for water of finite depth that satisfies the water free surface condition, the flat seabed boundary condition and the boundary at infinity (Linton, 1999), and it is given by:

$$G(\mathbf{x},\boldsymbol{\xi})=-\sum_{m=0}^{\infty}\frac{K_0(k_mR)}{\pi H\left(1+\dfrac{\sin 2k_mH}{2k_mH}\right)}\cos k_m(z+H)\cos k_m(\zeta+H) \tag{22}$$

where k_m is a positive root number satisfying the equation $k_m\tanh(k_mH) = -\omega^2/g$ with $m \geq 1$ and $k_0 = ik$, K_0 is the modified Bessel function of the second kind, and R is the horizontal distance between **x** and **ξ**.

In the computation of the coupled plate-water motion, the governing equation for the equivalent Mindlin plate is solved using the standard FE method. The floating plate is discretised into a finite number of 8-node Mindlin plate elements, as shown in Figure 19 (a). Note that 8-node Mindlin plate elements are able to provide more accurate results as compared to the 4-node elements as their shape functions are of higher order (Tay et al., 2007). For the fluid domain, only the wetted surface S_{HB} needs to be discritized into elements according to the boundary element method procedure. The hydroelastic responses computed from the hybrid FE-BE method were found to be in very good agreement with experimental test results. Details of numerical implementation and validation of the numerical results are given in Nguyen et al. and Wang et al.'s work (Nguyen et al., 2018; Nguyen and Wang, 2020; Wang and Tay, 2011), and are not presented again in this paper for brevity.

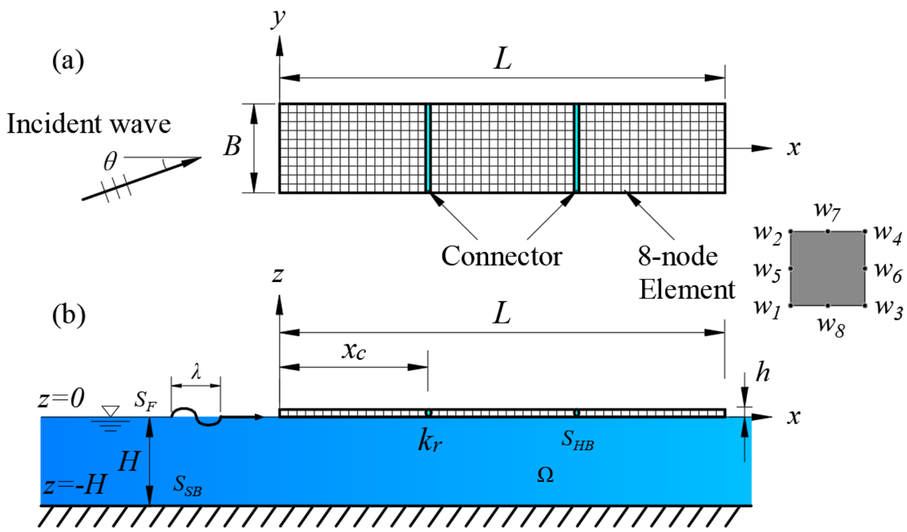

Figure 19. Schematic Diagram of Coupled Plate–Water Problem with the Hybrid FE-BE Method: (a) Plan View and (b) Elevation View.

4.2 Response of Large Floating Structures Composed of Rectangular Modules

Figure 20 shows the dimensions of floating structures to be analyzed. Selected floating structures are composed of rectangular modules (30 m × 15 m × 5 m) with aspect ratios ranging from 1.0 to 4.0. The regular incoming wave periods vary from 2 s to 20 s, and three incident wave directions of 0°, 45° and 90° are considered in the analysis.

Figure 21 presents hydroelastic responses of the large floating structure (120 m × 60 m in plan dimensions) rigidly interconnected with rectangular floating modules in regular wave conditions with incident wave period of 8 s and wave angle of 0°. Symbol, A, in the y axis indicates the wave amplitude which is half of the wave height. It is seen that the critical vertical deflections occur at the fore and aft, while the maximum bending moment occurs in the mid-span of the entire structure. By capturing peak points of each case, critical deflections and flexural stresses corresponding to different wave periods are inferred for rectangular and square floating structures, as shown in Figures 22 and 23. Note that the flexural stress σ_n is computed from $\sigma_n = M_n\, y \,/\, I$, where M_n is the bending moment, y is the distance of the top/bottom slab from the neutral axis and I is the area moment of inertia. Red, blue and grey solid lines represent the hydroelastic responses when exposed to incident wave angles of 0°, 45° and 90°, respectively. It is evident that critical vertical deflections and flexural stresses vary with respect to the incident wave period and direction.

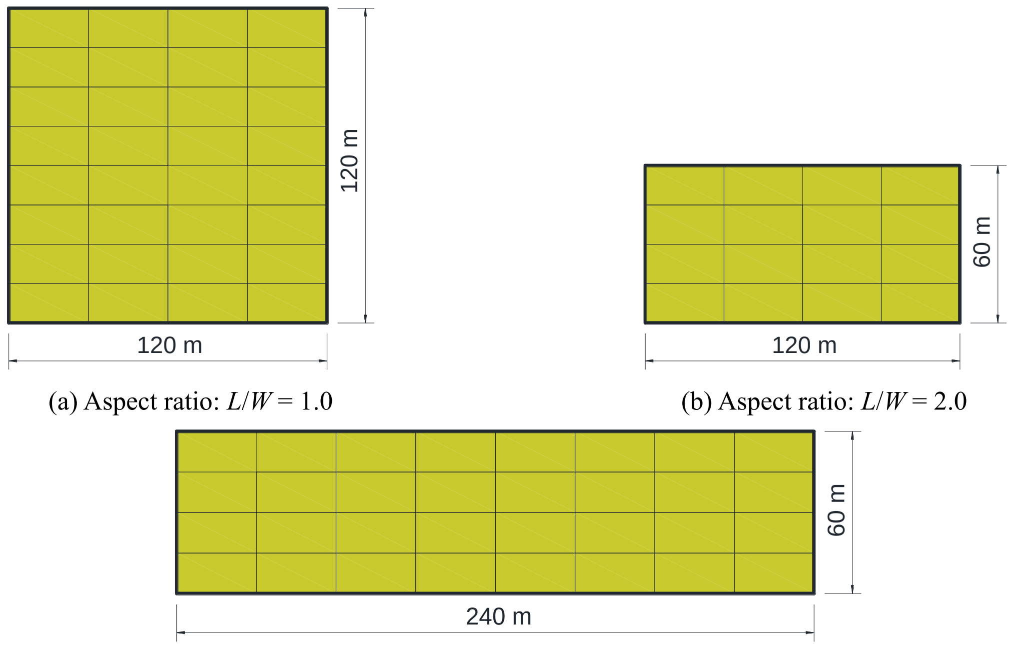

(a) Aspect ratio: $L/W = 1.0$

(b) Aspect ratio: $L/W = 2.0$

(c) Aspect ratio: $L/W = 4.0$

Figure 20. Dimensions of Floating Structures Composed of Rectangular Modules.

For rectangular floating structures (120/240 m × 60 m), maximum deflection occurs at a lower wave period in the beam sea condition as compared to head sea and oblique wave conditions, while this phenomenon is not clearly observed in the square floating structure (120 m × 120 m). As for flexural stresses, regular wave loads generally induce higher stress in the longitudinal direction than in the transverse direction for rectangular floating structures. The maximum stress value usually increases with the aspect ratio, and it can reach up to around 15 MPa when the aspect ratio is 4.0, which needs to be handled with caution in design. Also, a longish floating structure may sustain larger bending loads as compared to a floating structure with a smaller length-to-width ratio. In addition, wave obliqueness may result in different stress distribution at corresponding critical incident wave period. Specifically, maximum stresses occur at a lower wave period in the oblique wave condition than those in the head sea condition.

Past research work showed that a large-scale monolithic structure is subjected to enormous wave-induced bending loads, which may result in structural failure due to insufficient strength (Gao et al., 2011; Riggs and Ertekin, 1993; Watanabe et al., 2004). Under such circumstances, multi-module floating structures with internal hinge connections may be used to reduce flexural stresses (Teng et al., 2014; Yoon et al., 2014; Zhao et al., 2015). Herein, the hybrid BE-FE analyses with the consideration of hinge joints are also performed on the large floating structure composed of rectangular floating modules. Figure 24 shows vertical deflection and bending moment profiles of rectangular floating modules connected with hinge joints. The dimensions of the entire structure and wave characteristics are identical to the case presented in Figure 21. As compared to the rigid-interconnected floating structure system, the use of hinge joints can significantly reduce the moment magnitude, and the maximum values occur at mid-points between two hinges. Meanwhile, the critical deflections take place at both free ends and hinge location, and the critical values increase from 0.6 m to 1.5 m, which might be not acceptable in practice. Therefore, a trade-off needs to be considered between internal loads and structure motions in the conceptual design of a floating structure system.

Figure 25and Figure 26 compare the hydroelastic responses of hinge-interconnected (dash lines) and rigid-interconnected (solid lines) floating structures with different aspect ratios. In general, the existence of hinge joints significantly reduces the flexural stresses in both directions, but increases the vertical deflections to some extent. Particularly, maximum deflections of hinge-connected structures occur at lower incident wave periods compared to those of rigid-connected structures. The variation of maximum deflection with the wave periods is quite similar among hinge-connected structures with different aspect ratios, which attributes to the samedimensions of individual modules. For multi-modular floating structures connected with hinges, flexural stresses are quite small, but deflections become significant. In such a condition, flexible connections with certain rotational stiffness values may be viable to balance the load and motion response of large floating structures.

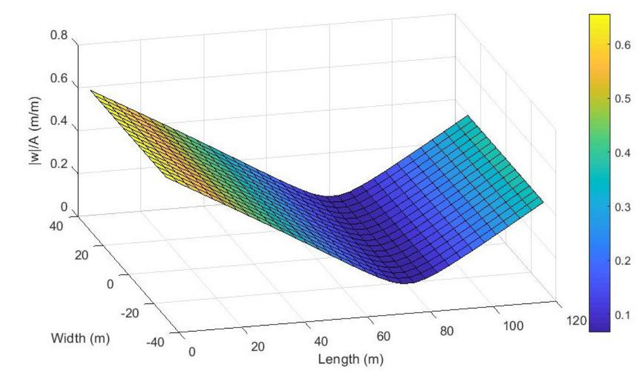

(a) Vertical deflection

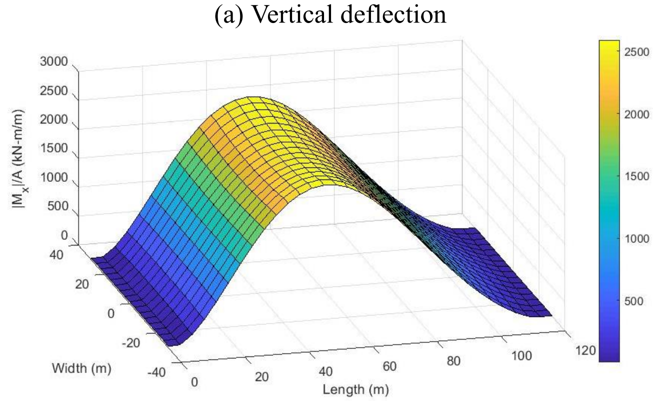

(b) Bending moment

Figure 21. Hydroelastic Responses of the Large Floating Structures (120 m × 60 m) Composed of Rigid-Connected Rectangular Modules in a Head Sea (T = 8 s).

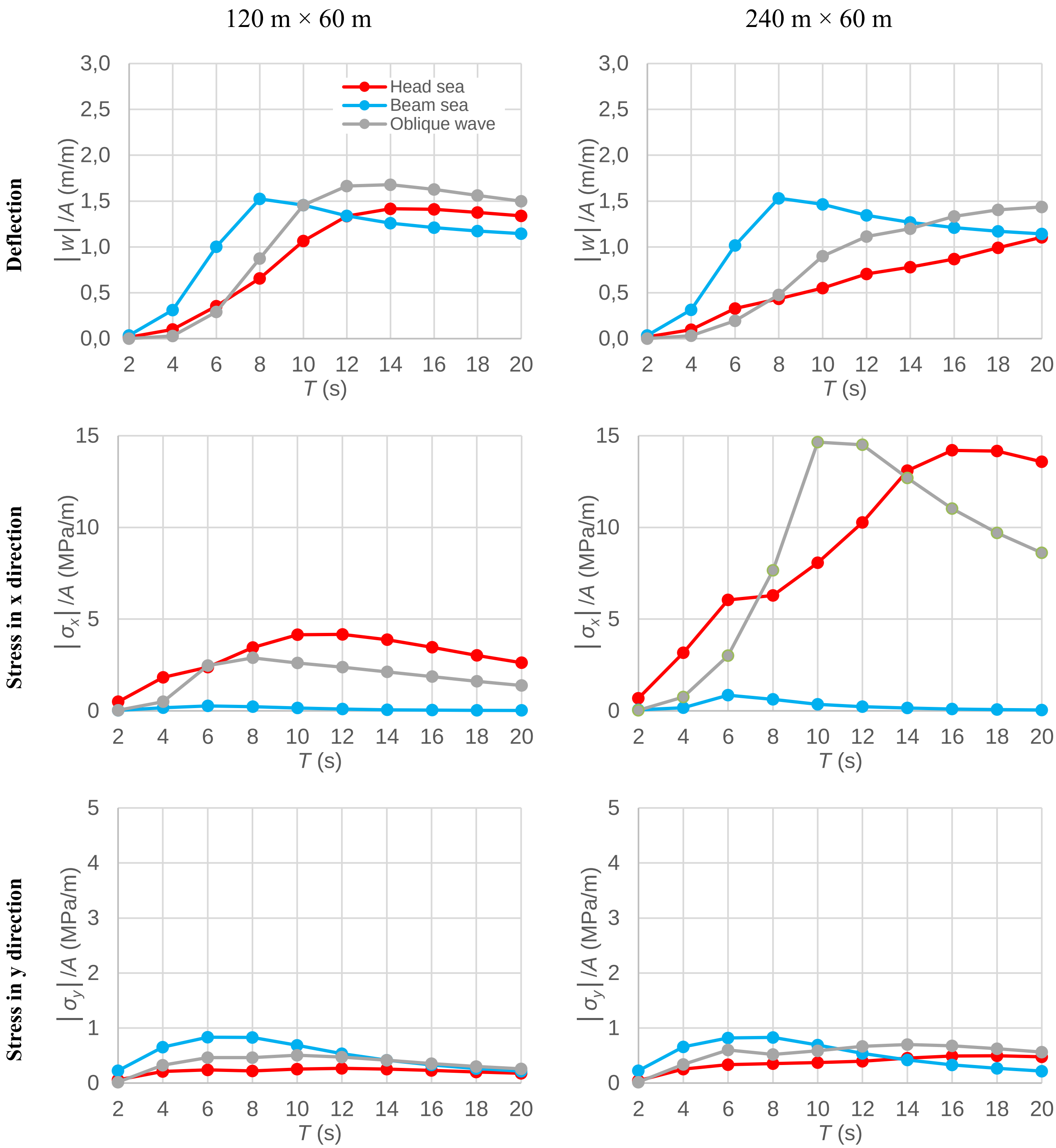

Figure 22. Variation of Maximum Vertical Deflections and Flexural Stresses of Rigid-Connected Rectangular Floating Structures (120/240 m × 60 m) as a Function of Incident Wave Periods.

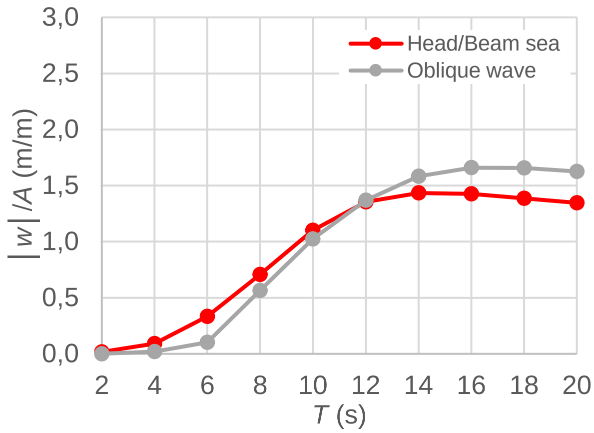

Deflection

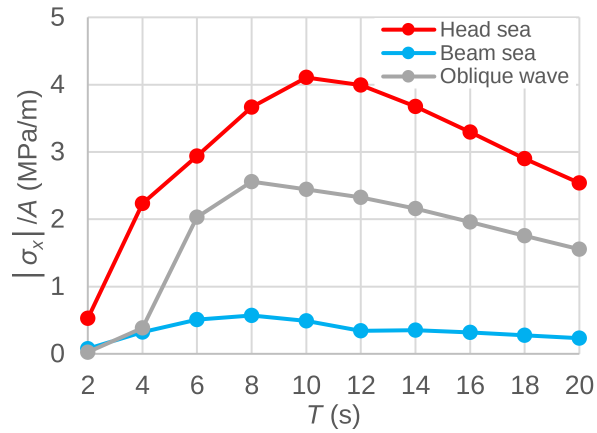

Stress

Figure 23. Variation of Maximum Vertical Deflections and Flexural Stresses of Rigid-Connected Square Floating Structures (120 m × 120 m) as a Function of Incident Wave Periods.

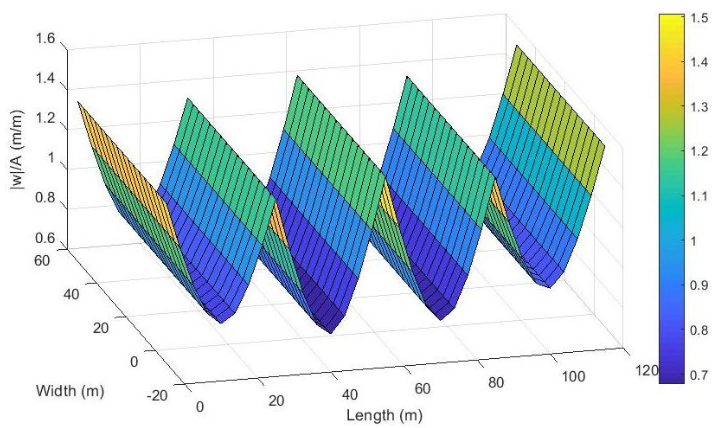

(a) Vertical deflection

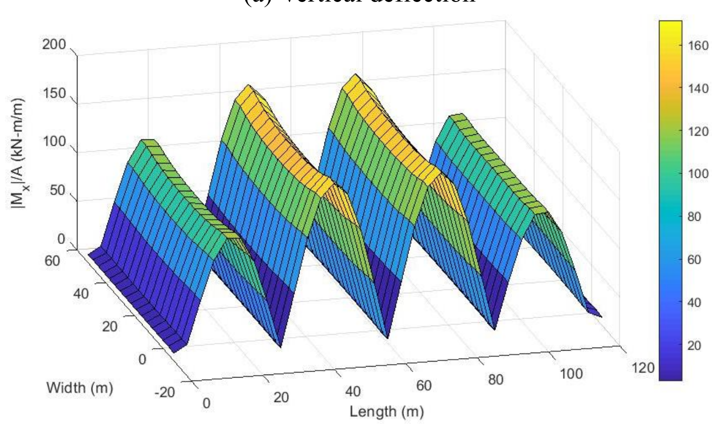

(b) Bending moment

Figure 24. Hydroelastic Responses of the Large Floating Structures (120 m × 60 m) Composed of Hinge-Connected Rectangular Modules in a Head Sea (T = 8 s).

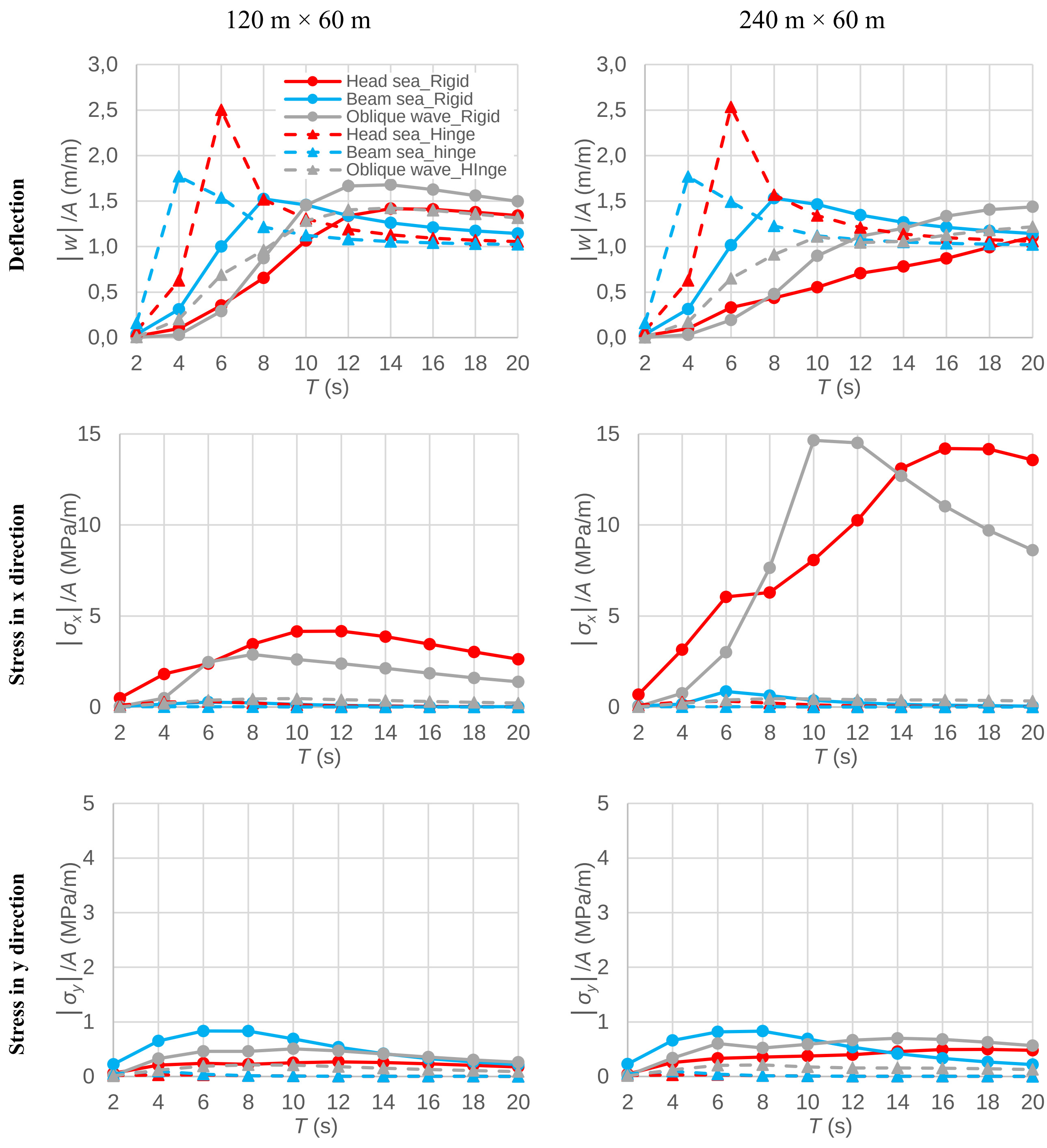

Figure 25. Variation of Maximum Vertical Deflections and Flexural Stresses of Hinge-Connected Rectangular Floating Structures (120/240 m × 60 m) as a Function of Incident Wave Periods.

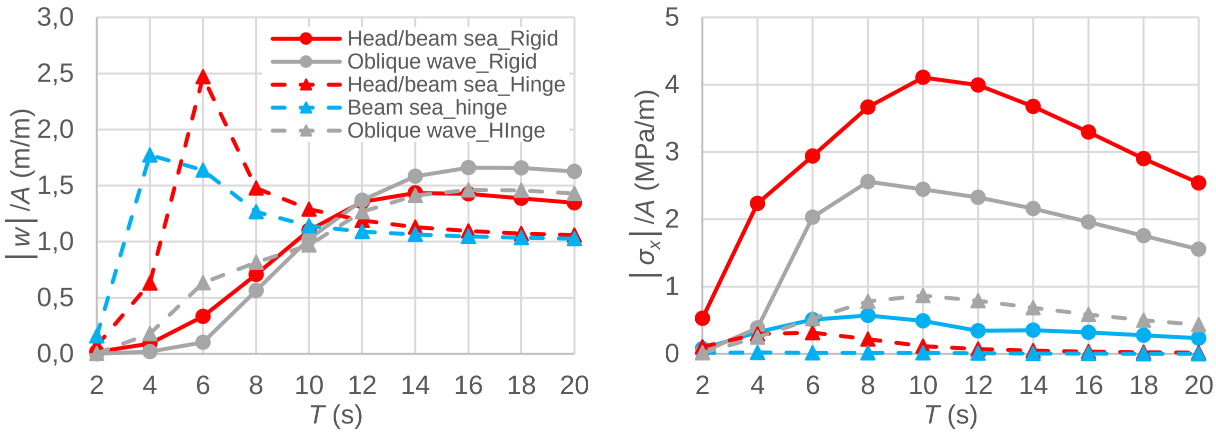

Deflection **Stress**

Figure 26. Variation of Maximum Vertical Deflections and Flexural Stresses of Hinge-Connected Square Floating Structures (120 m × 120 m) as a Function of Incident Wave Periods.

4.3 Response of Large Floating Structures Composed of Hexagonal Modules

Figure 27 shows dimensions of three floating structures with hexagonal modular units. In the hydroealstic analysis, the same incident wave periods and obliqueness as described in Section 4.2 are considered. Figure 28 presents the hydroelastic response of a specific floating structure (137.4 m × 66 m) rigidly interconnected with hexagonal modules in a head sea (T = 8s). The deflection profile and magnitude are quite similar to those of rectangular floating structures (120 m × 60 m) as shown in Figure 21. However, moment concentration is observed at two longitudinal jagged edges formed by hexagonal modules, resulting in much larger flexural stresses.

Figures 29 and 30 compare the critical vertical deflection and bending moment between various floating structures composed of hexagonal modules (dash lines) and rectangular modules (solid lines). While deflection curves are similar to each other, flexural stress magnitudes are much larger for hexagonal-modular floating structures due to the concentration of moment at the jagged edges. However, the wave periods corresponding to the critical flexural stress values are almost the same for floating structures composed of rectangular and hexagonal shape modules. The use of hinge joints is more complicated in hexagonal-modular floating structures due to various layout of connecting lines, and it will be discussed in future studies.

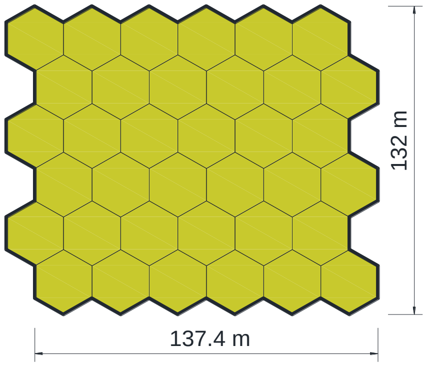

(a) Aspect ratio: $L/W = 1.04$

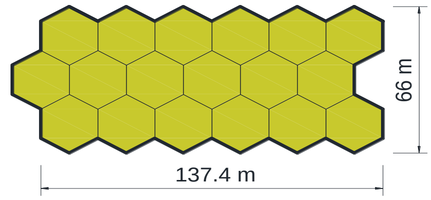

(b) Aspect ratio: $L/W = 2.08$

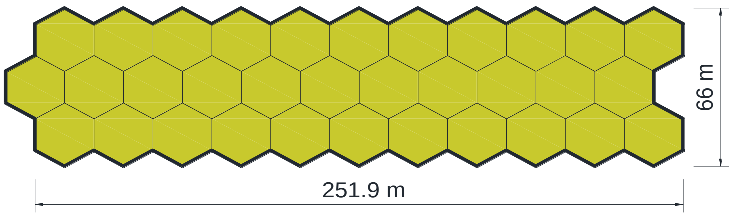

(c) Aspect ratio: $L/W = 3.82$

Figure 27. Dimensions of Floating Structures Composed of Hexagonal Modules.

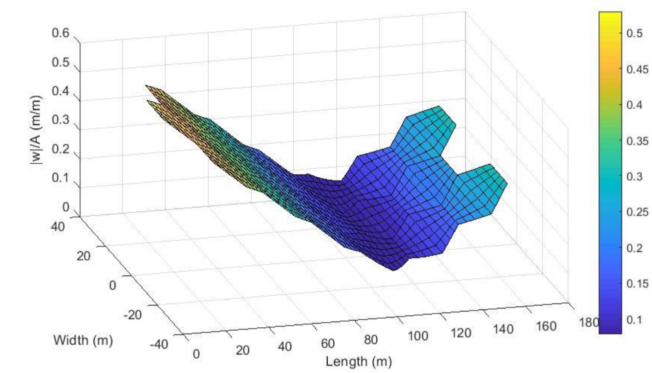

(a) Vertical deflection

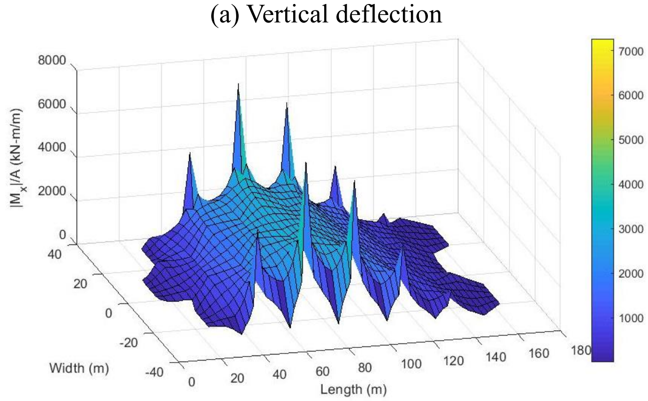

(b) Bending moment

Figure 28. Hydroelastic Responses of the Large Floating Structures (137.4 m × 66 m) Composed of Rigid-Connected Hexagonal Modules in a Head Sea (T = 8 s).

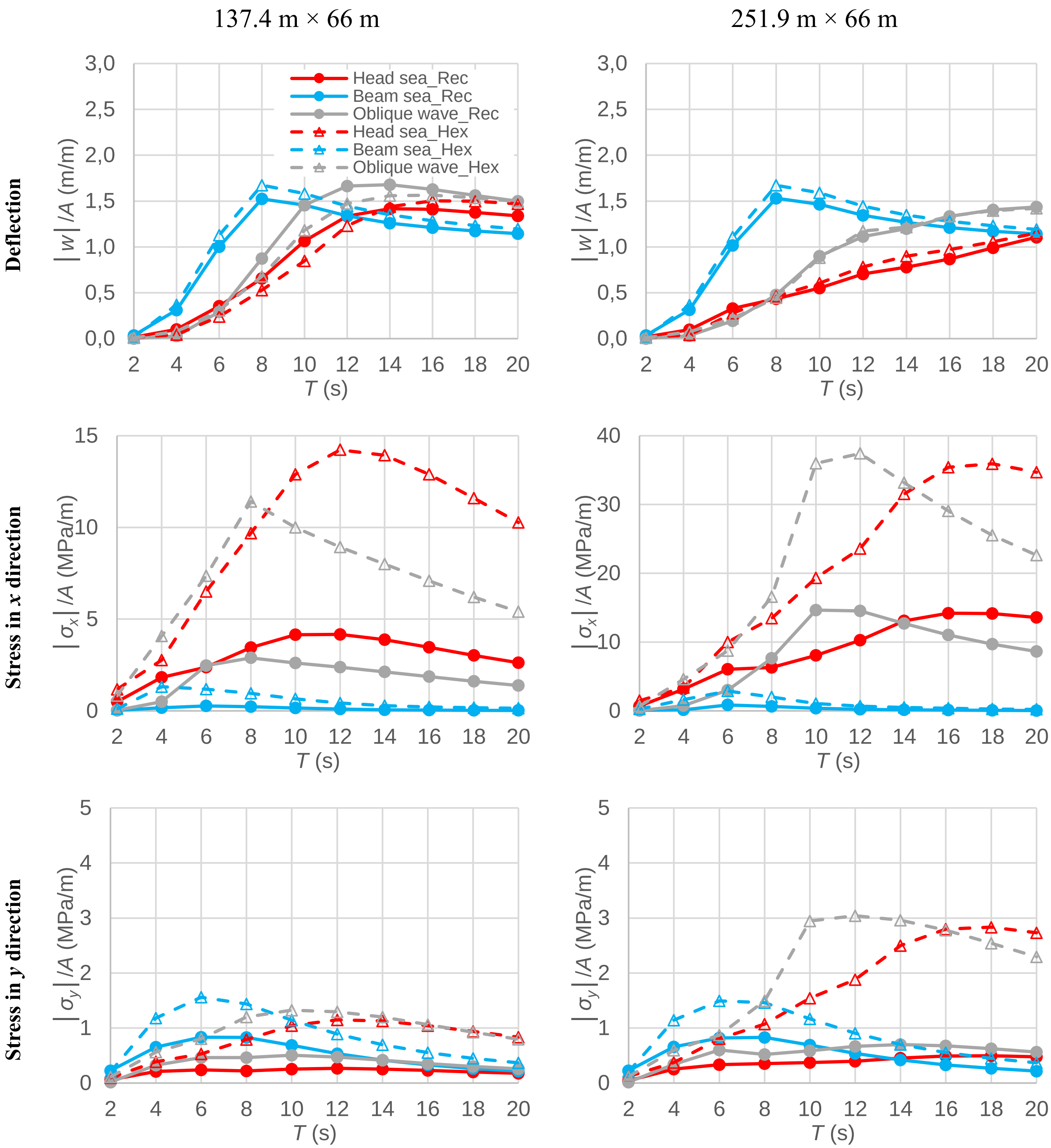

Figure 29. Variation of Maximum Vertical Deflections and Flexural Stresses of Large Floating Structures (137.4/251.9 m × 66 m) Composed of Rigid-Connected Hexagonal Modules as a Function of Incident Wave Periods.

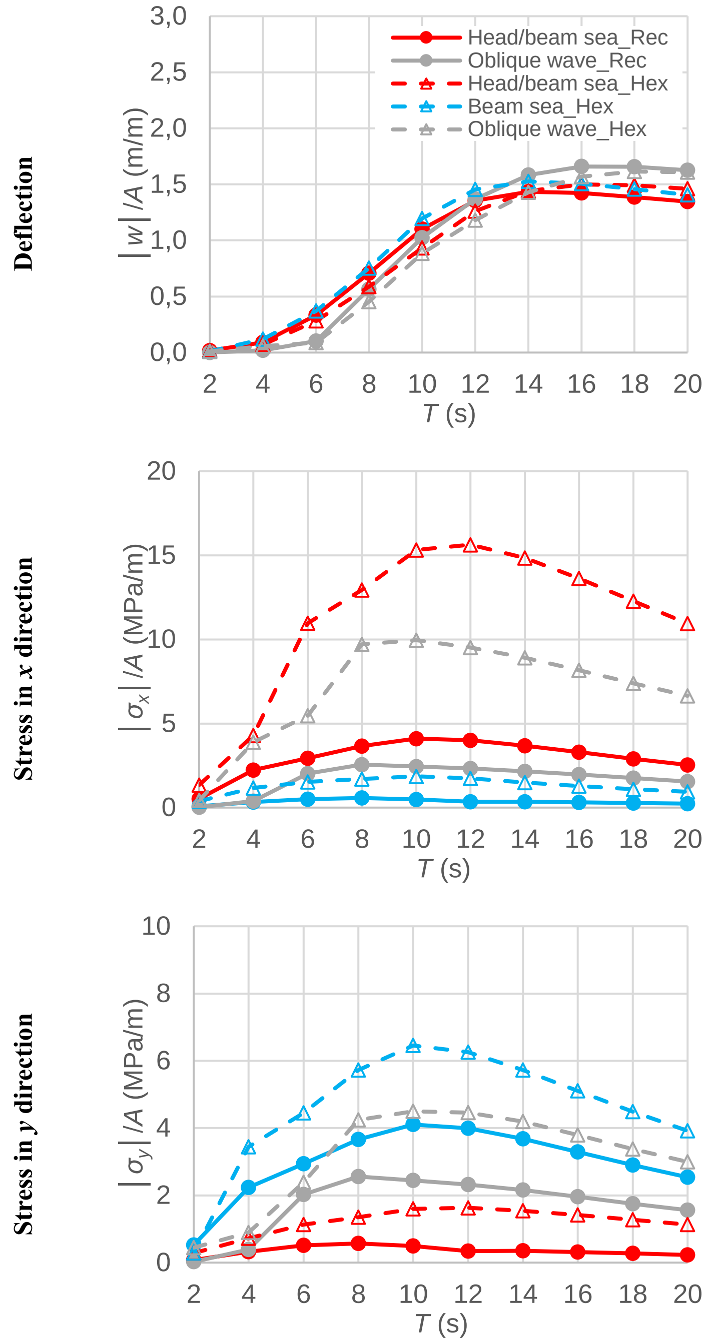

Figure 30. Variation of Maximum Vertical Deflections and Flexural Stresses of Large Floating Structures (137.4 m × 132 m) Composed of Rigid-Connected Hexagonal Modules as a Function of Incident Wave Periods.

5. CONCLUSIONS AND RECOMMENDATIONS

A variety of box-like structural solutions are considered as alternatives for floating modules. FE analysis approach was utilized to investigate the structural performance of various design alternatives, and the effects of geometrical shapes, cell numbers and slab thickness were investigated. Preliminary prestressing designs were further explored on the basis of the analysis results. In addition, material requirements for different configurations are compared to determine the most economical solution for concrete floating modular units. Also, the global response of large floating structures comprising the recommended modular structures with different geometrical shapes was investigated by performing hydroelastic analysis with self-developed hybrid BE-FE code. Based on the analysis results, the following conclusions may be drawn:

1. For box-like structures, the tensile stresses reduce with an increase in slab/wall thickness and decrease of span length between two wall supports. The existence of interior walls is beneficial in increasing the flexural rigidity and can therefore significantly reduce the tensile stresses. Except for 300 mm thick wall/slab 6-cell hexagonal and 24-cell hexagonal module, all box-like modular structures calls for the provision of prestressing steels.

2. Based on close evaluations, it is preferable to choose 150 mm thick wall/slab 2-cell PC rectangular module and 150 mm thick wall/slab 6-cell PC hexagonal module as preferable structural solutions. Although the material costs of 24-cell hexagonal module is the lowest among all box-like structures, its complex configuration makes the construction procedure time-consuming and costly.

3. The global hydroelastic response of floating structures comprising modular units varies with the aspect ratio and incident wave characteristics. Regular wave loads generally induce more significant flexural stresses in the longitudinal direction than those in the transverse direction, and this should be handled with caution when the aspect ratio of the structure is large.

4. The use of hinge joints can significantly reduce the bending moments, but relatively increase the critical vertical deflections. A trade-off needs to be considered between internal loads and structure motions in the conceptual design of a floating structure system. Further studies on the exploration of optimal flexible connection stiffness values needs to be conducted to achieve economical large floating structure solutions with acceptable deflection and stress responses.

5. Moment concentration is observed at longitudinal jagged edges formed by hexagonal modules, resulting in much larger flexural stresses. It is suggested to adopt smooth-shaped sides for the application of large floating structure systems.

ACKNOWLEDGEMENT

The authors gratefully acknowledges the funding supports from Natural Science Foundation of Jiangsu Province under Grant No. BK20180487 and National Natural Science Foundation of China (NSFC) under Grant No.51808292

REFERENCES

Ang K.K., Dai J., Zhang C. Research and development of new spaces on the sea for industrial and recreational applications. In: Proceedings of the International Conference on Sustainable Civil Engineering and Architecture. Springer Nature, Singapore; 2020.

Dai, J , Wang, C.M., Utsunomiya, T., and Duan, W. Review of recent research and developments on floating breakwaters. *Ocean Engineering*, 2018;158:132-151.

Dai, J., Zhang, C., Lim, H. V., Ang, K. K., Qian, X., Wong, J. L. H., ... & Wang, C. L. Design and construction of floating modular photovoltaic system for water reservoirs. Energy. 2020. 191, 116549

Fernandez R.P., Pardo M.L. Offshore concrete structures. *Ocean Engineering*. 2013;58:304-16.

Fu, S., Moan, T., Chen, X., and Cui, W., 2007. Hydroelastic Analysis of flexible floating interconnected structures. *Ocean Eng.* 34:1516–31.

Gao, R.P., Tay, Z.Y., Wang, C.M. and Koh, C.G. Hydroelastic response of very large floating structure with a flexible line connection. *Ocean Engineering*. 2011;38:1957-66.

Jiang, D., Tan, K. H., Dai, J., Ong, K. C. G., and Heng, S. Structural performance evaluation of innovative prestressed concrete floating fuel storage tanks. *Structural concrete*, 2019, 20(1):15-31.

Jiang, D. Tan, K.H., Ong, K.C.G., Heng, S., Dai, J., Lim, B.K., and Ang, K.K. Behavior of prestressed concrete self-stabilizing floating fuel storage tanks. In: Proceedings of the 4th Congrès International de Géotechnique - Ouvrages -Structures. CIGOS 2017. pp 1097-1106.

Jiang D, Tan, K.H., Wang, C.M., Ong, K.C.G., Bra, H., Jin, J., and Kim, M. Analysis and design of floating prestressed concrete structures in shallow waters. *Marine Structures*. 2018;59:301-320.

Koh, H. S., & Lim, Y. B. The floating platform at the Marina Bay, Singapore, Structural Engineering International: Journal of the International Association for Bridge and Structural Engineering, 2009; 19(1):33-37.

Lamas-Pardo, M., Iglesias, G., & Carral, L.. A review of very large floating structures (VLFS) for coastal and offshore uses. Ocean Engineering, 2015. 109, 677-690.

Linton CM. Rapidly convergent representation for Green's functions for Laplace's equation. Proc R Soc Lond 1999;A(455):1767–97.

Loukogeorgaki, E., Michailides, C. and Angelides, D., 2012. Hydroelastic analysis of a flexible mat-shaped floating breakwater under oblique wave action. *J Fluid Struct*. 31:103-24.

Mcallister K. Mobile offshore bases—An overview of recent research. *Journal of Marine Sciences and Technology*. 1997;2:173-181.

Morris R.D. Artificial floating island. US patent no.5421282; 1996.

Nguyen, H.P., Dai, J., Wang, C.M., Ang, K.K., and Luong, V.H. Reducing hydroelastic response of a VLFS using vertical elastic mooring lines. *Mar Struct*. 2018;59:251–70.Nguyen, H.P., Wang, C.M. Heaving wave energy converter-type attachments to a pontoon-type very large floating structure. *Eng. Struct.* 2020; 219:110964.

NUS, SINTEF. Modular multi-purpose floating structures: structural analysis and design of MMFS modules. Technical report no. 21 submitted to JTC; 2019.

Priedeman, J.S., Anderson, T.R. Floating concrete structures. *Concrete International*. 1985; .7(8), 3.

Ramsamooj, D. V. and Shugar, T. A. Reliability analysis of fatigue life of the connectors-the US mobile offshore base. *Marine Structures*. 2002;15:233–250.

Ren, N., Zhang, C. Magee, A.R., Hellan, O., Dai, J., and Ang, K.K. Hydrodynamic analysis of a modular multi-purpose floating structure system with different outermost connector types. *Ocean Engineering*. 2019, 176:158-168.

Riggs, H.R., and Ertekin, R.C. Approximate methods for dynamic response of multi-module floating structures. *Marine Structures*. 1993; 6: 117-141.

Rognaas G, Xu, J., Lindseth, S., and Rosendahl, F. Mobile offshore base concepts concrete hull and steel topsides. *Marine Structures*. 2001;14:5-23.

Seasteading Institute. Floating City Project. 2019. In: https://www.seasteading.org/floating-city-project/ (July 12, 2020).

Tay, Z. Y., Wang, C. D., & Wang, C. M. Hydroelastic response of a box-like floating fuel storage module modeled using non-conforming quadratic-serendipity Mindlin plate element. Engineering structures. 2007, 29(12), 3503-3514.

Tay, Z.Y., Wang, C.M. and Utsunomiya, T., Hydroelastic responses and interactions of floating fuel storage modules placed side-by-side with floating breakwaters. Marine structures, 2009, 22(3), pp.633-658.

Teng, B.. Gou, Y., Wang, G. and Cao, G. Motion response of hinged multiple floating bodies on local seabed. *Proceedings of the Twenty-Fourth International Offshore and Polar Engineering Conference (ISOPE 2014)*. Busan, South Korea 2014; 591-8.

Utsunomiya T, Watanabe E, Eatock Taylor R. Wave response analysis of a box-like VLFS close to a breakwater. In: Proc. of 17th int. conf. on offshore mech. and artic engrg. 1998. OMAE98-4331

Wan, L., Jiang, D., and Dai, J. Numerical modelling and dynamic response analysis of curved floating bridges with a small rise-span ratio. *J. Mar. Sci. Eng.* 2020, 8, 467.

Wang C.M., Wang, B.T. Large floating structures: technological advances. Singapore: Springer Singapore; 2015.

Wang C.M., Tay Z.Y. Hydroelastic Analysis and Response of Pontoon-Type Very Large Floating Structures. In: Bungartz HJ., Mehl M., Schäfer M. (eds) Fluid Structure Interaction II. Lecture Notes in Computational Science and Engineering, vol 73. Springer, Berlin, Heidelberg; 2011.

Wang, C.M., and Tay, Z.Y. Very large floating structures: applications, research and development. *Procedia Engineering*. 2011; 14:62-72.

Watanabe E, Utsunomiya, T., and Wang, C. M. . Hydroelastic analysis of pontoon-type VLFS: a literature survey. *Engineering structures*. 2004; 26:245-56.

Yee, A.A. Design and construction of composite precast prestressed concrete structures on land and sea. Keynote Paper in the 11th Arab structural engineering conference, KFUPM, Dhahran, Saudi Arabia, October 25–27, 2009.

Yoon, J., Cho, S., Jiwinangun, R. G., and Lee, P. Hydroelastic analysis of floating plates with multiple hinge connections in regular waves. *Marine Structures*. 2014; 36:65-87.

Zhao, C., Hao, X., Liang, R., and Lu, J. Influence of hinged conditions on the hydroelastic response of compound floating structures. *Ocean Eng*. 2015; 101:12-24.